WYOMING STATE GEOLOGICAL SURVEY
Thomas A. Drean, Director and State Geologist
Laramie, Wyoming

Interpreting the past, providing for the future

OPEN FILE REPORT 2016-4
Ervay Basin SW 1:24,000-scale Bedrock Geologic Map

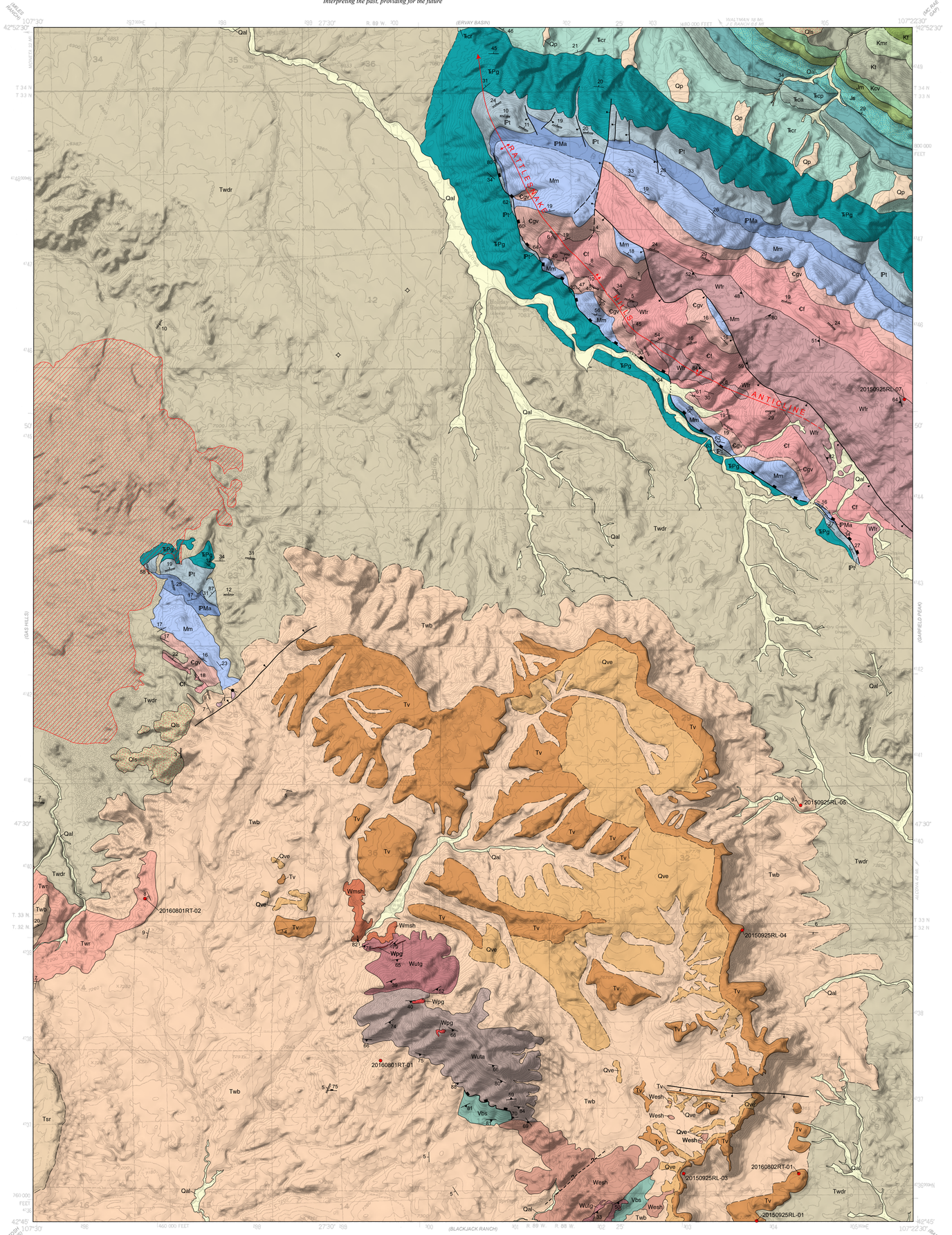

CORRELATION OF MAP UNITS

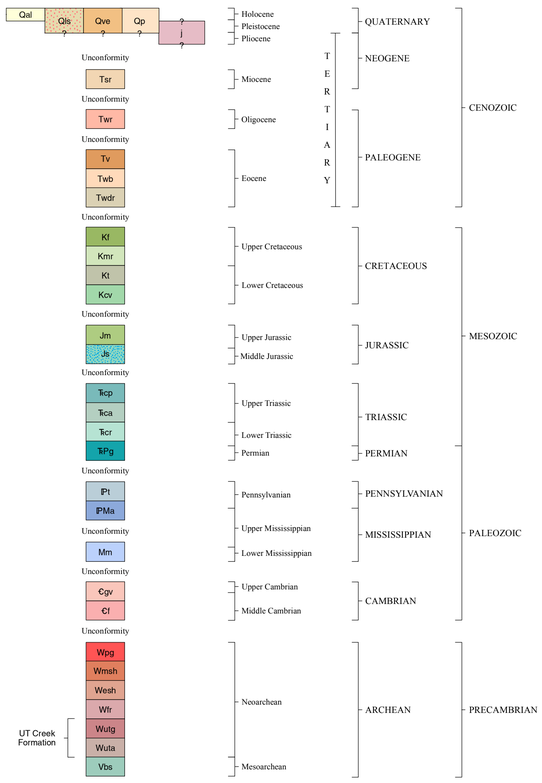

MAP SYMBOLS

Definitions: *Certain—Estimated location <25 m*
Approximate—Estimated location 25-100 m
Inferred—Estimated location >100 m

Formation contact—Continuous where certain; long dash where approximate; short dash where inferred

Fault—Continuous where certain; long dash where approximate; short dash where inferred; dotted where concealed; queried where identity or existence uncertain; rectangle on upthrown block of reverse fault; bar and ball on downthrown block of normal fault

Anticline—Continuous where certain; long dash where approximate; arrow on end of axis indicates direction of plunge

Overturned anticline—Continuous where certain

27 **Strike and dip of inclined bedding**

75 **Strike and dip of overturned bedding**

33 **Strike and dip of inclined bedding in cross-bedded rocks**

50 **Strike and dip of foliation**

84 **Strike and dip of joint**

Strike of vertical joint

20150925RL-01 **Sample location**—Showing sample number (refer to accompanying report for analyses)

Oil or gas well, dry hole

Reclaimed and graded area—Extensive amount of mapped geologic unit has been removed

EXPLANATION

DESCRIPTION OF MAP UNITS

Cenozoic

Qal **Alluvium (Holocene)**—Unconsolidated to poorly consolidated sand, silt, clay, coarse gravels, and cobbles, mainly along local intermittent stream courses; locally intermixed with colluvium. Thickness less than 8 m (26 ft)

Qls **Landslide debris (Holocene and Pleistocene[?])**—Blocks and slumps of locally derived bedrock from steep and unstable slopes; most common in Cloverly Formation as well as Wagon Bed Formation along Beaver Rim. Thickness less than 122 m (400 ft)

Qve **Volcanic eluvium (Holocene and Pleistocene[?])**—Unconsolidated remnants derived from in situ weathering of Rattlesnake Hills volcanic rocks; grades into Rattlesnake Hills volcanics and volcanic conglomerates within Wagon Bed Formation. Thickness less than 3 m (10 ft)

Qp **Pediment deposits (Holocene and Pleistocene[?])**—Unconsolidated subangular pebble and cobble gravels in a coarse sandy matrix of locally derived sedimentary rocks. Thickness less than 3 m (10 ft)

j **Jasper, jasperoid (Pleistocene[?] and Pliocene[?])**—Jasperoid of unknown genesis, orange to red, weakly bedded. Thickness not determined

Tsr **Split Rock Formation (Miocene)**—Interbedded sandstone and conglomerate; not exposed in outcrop but inferred as the lower porous sandstone sequence from Cola and Sutherland (2014). Thickness less than 30 m (100 ft)

Twr **White River Formation (Oligocene)**—White well-indurated silty sand and whitish-tan reworked ash with fine- to medium-grained lithic fragments; contains abundant biotite and glass shards, along with persistent thin pumicite beds (Love, 1970). Disconformable basal contact scours into the underlying Wagon Bed Formation. Occurs only on the northwestern edge of Beaver Rim. Thickness approximately 0–49 m (160 ft)

Tv **Rattlesnake Hills volcanic rocks, undifferentiated (Eocene)**—Volcanic flows, breccias, and agglomerates associated with the Rattlesnake Hills volcanics range in composition from phonolite (Hoch, 1991) to trachyte to dacite; interfingers with Wagon Bed Formation. U-Pb zircon geochronology from topographically highest outcrop yields 45.2 ± 0.2 Ma. Thickness less than 6 m (20 ft)

Twb **Wagon Bed Formation (Eocene)**—Three distinct facies exist in map area. Conglomerate contains cobbles and pebbles of predominately Rattlesnake Hills volcanics, UT Creek Formation, and Sacawee orthogneiss, with unconsolidated boulders as large as 2 m (7 ft) in diameter. Tuffaceous siltstone and claystone are whitish gray, poorly consolidated to well indurated, and rarely exposed except for one brilliant white outcrop on the west side of Black Mountain. Lapilli tuff is a white to light-gray fine-grained and poorly consolidated well-indurated ash with larger clasts of glass and feldspar and ash-rich clasts up to 15 cm (6 in). U-Pb zircon geochronology of Wagon Bed tuffs yields ages of 47.9 ± 0.3 and 45.4 ± 0.2 Ma. Basal contact is disconformable; interfingers with Rattlesnake Hills volcanics. Thickness is highly variable with a maximum of 122 m (400 ft)

Twdr **Wind River Formation (Eocene)**—Variegated yellowish-brown to orange claystone, siltstone, sandstone, and conglomerate interbedded with white tuffs (Love, 1970); sandstones are arkosic, medium to coarse grained with an abundance of angular quartz grains; conglomerates are predominately comprised of Precambrian igneous and metamorphic cobbles. Basal contact is disconformable. Thickness is highly variable but generally less than 300 m (1,000 ft)

Mesozoic

Kf **Frontier Formation, main body (Upper Cretaceous)**—Interbedded siltstone, black shale, and gray to brown, fine- to coarse-grained sandstone. Middle and lower sand beds are fine to medium grained, well sorted with rounded grains; subangular dark lithics give sandstones a 'salt and pepper' appearance. Sandstones create small ridges between less resistant shales, siltstones, bentonites, and coals. Overlain by Wall Creek Sandstone Member, not exposed on map. Basal contact is conformable and sharp. Thickness approximately 204 m (670 ft) (Bogrett, 1951)

Kmr **Mowry Shale (Upper Cretaceous)**—Organic, black to dark-gray, siliceous shale that contains abundant fish scales and numerous bentonite beds. Bedding and laminations are usually less than two centimeters thick. Weathers silver gray and forms prominent slopes and resistant ridges. Basal contact is conformable (Roth, 1955). Thickness is 116 m (380 ft) (Bogrett, 1951)

Kt **Thermopolis Shale (Lower Cretaceous)**—Nonresistant, dark-gray to black, fissile, bioturbated shale and siltstone that is noncalcareous and carbonaceous; occasional thin resistant siltstones and sandstones throughout; iron concretions are present near the top (Pekarek, 1978). Base is conformable. Approximately 58 m (190 ft) thick (Bogrett, 1951)

Kcv **Cloverly Formation (Lower Cretaceous)**—Resistant buff to gray, brown-weathering, quartz and chert pebble conglomerate with rounded pebbles and granules at base, variegated shale and claystone in middle, and capped by a fine-grained cross-bedded, slabby sandstone and locally by a white recrystallized limestone. The conglomeratic unit forms a ridgetop in the mapped area; commonly broken by landslides. Basal contact is unconformable. Thickness is approximately 21 m (70 ft) (Bogrett, 1951)

Jm **Morrison Formation (Upper Jurassic)**—Dominated by variegated calcareous red to purple shales and siltstones interbedded with buff, very fine to fine-grained, cross-bedded sandstone channels. The shales weather gray green and form slopes below the Cloverly Formation ridges. Basal contact is gradational in mapped area (Wroble, 1953). Thickness is approximately 64 m (210 ft) (Pekarek, 1977)

Js **Sundance Formation (Upper and Middle Jurassic)**—Consists of a basal buff to gray, fine-grained, partially glauconitic, calcite-cemented, cross-bedded sandstone; overlain by a nonresistant, thinly bedded fine-grained sandstone interbedded with red and gray calcareous shales. Upper section is dominated by pale-green to olive-green shales and thinly laminated siltstones, glauconite, ooids, and limey sands. Abundant fossil hash and belemnites occur throughout the formation but decrease in abundance below the uppermost glauconitic layer. The bulk of the formation is a slope former, except for the lower sandstones which crop out in low ridges. Basal contact is erosional and unconformable. Thickness 111 m (365 ft) (Pekarek, 1977)

Chugwater Formation (Triassic)

Tcp **Popo Agie Member**—Red, calcareous shale and siltstone with very fine to fine-grained, subrounded, very well sorted, tan to white and red sandstone lenses. Moderately resistant sand lenses less than 0.6 m (2 ft) thick weather gray to dark gray and are commonly capped by ripple marks. Red siltstones are nonresistant and calcareous, and weather to orange-red soils. Exposed in valley bottoms. Basal contact is conformable (Wroble, 1953). Thickness is approximately 91 m (300 ft) (Bogrett, 1951)

Tca **Alcova Limestone Member**—Pinkish-gray to purple micritic limestone, thinly bedded with undulating bedding planes and frequent stromatolites. Weathers to white with orange lichen. Typically forms resistent hogbacks along northeast limb of Rattlesnake Hills anticline. Basal contact is conformable. Thickness is approximately 6 m (20 ft) (Pekarek, 1977)

Tcr **Red Peak Member**—Interbedded reddish-orange to brick red shales, siltstones, and sandstone with minor thin gray to green beds of calcareous siltstones and shales. Forms gradual slopes and valleys below the Alcova Limestone Member. Basal contact is conformable (Paull and Paull, 1990). Thickness is approximately 241 m (790 ft) (Pekarek, 1977)

Mesozoic and Paleozoic

TPg **Goose Egg Formation (Lower Triassic and Permian)**—Sequence of pink to orangish-red, gypsum-rich shales and siltstones alternating with buff to gray to purple limestones and dolomites locally interbedded with thin chert layers. The members in descending order are Little Medicine Limestone Member, Freezeout Shale Member, Ervay Limestone Member, Difficulty Shale Member, Forelle Limestone Member, Glendo Shale Member, Minnekahta Limestone Member, and Opeche Shale Member (Paull and Paull, 1990). The limestones form prominent flatirons along the north end and northeast limb of the Rattlesnake Hills anticline. Basal contact is unconformable (Bogrett, 1951). Thickness is approximately 119 m (390 ft) (Pekarek, 1977)

Paleozoic

IPt **Tensleep Sandstone (Upper and Middle Pennsylvanian)**—Buff to tan, fine- to medium-grained, well-sorted, cross-bedded sandstone overlying a locally present white calcareous sandstone. Forms highly resistant ridges that weather peach gray. Fractures and quartz veins observed in altered zones. Basal contact is gradational (Burk, 1956). Thickness approximately 76 m (250 ft) (Pekarek, 1977)

IPMa **Amsden Formation (Lower Pennsylvanian and Upper Mississippian)**—Nonresistant buff to brick red to purple siltstone with minor layers of thin gray dolomite, limestone, and shale; a basal white to buff, very fine-grained, 6–9 m-thick (20–30 ft-thick) sandstone is equivalent to the Darwin Sandstone Member (Keefer and Van Leiu, 1966). Forms slopes and saddles between the more resistant Tensleep Sandstone and Madison Limestone, with an unconformable basal contact (Keefer and Van Lieu, 1966). Thickness is approximately 42 m (138 ft) (Bogrett, 1951)

Mm **Madison Limestone (Mississippian)**—Gray to bluish-purple microcrystalline to coarse-grained massive limestone. Includes minor buff to brown calcareous sand and silt layers, especially at base. Abundant chert nodules in various colors are present with banding and boudinage textures; locally mottled and fractured. Fossil shells occur locally. Typically exposed as resistant cliffs and ridges. Weathers to a reddish-brown soil. Basal contact is unconformable (Burk, 1956). Thickness is approximately 102 m (335 ft) (Bogrett, 1951)

Cgv **Gros Ventre Formation (Upper and Middle Cambrian)**—Nonresistant, white to buff, very fine to fine-grained, very well-sorted, platy thin sandstone layers interbedded with pale greenish-gray to reddish siltstone and shale with frequent dark silt lenses, and minor flat pebble conglomerate. Burrows present in glauconitic siltstones. Forms green, orange, and rust-colored soils and slopes. Thickness is approximately 85 m (280 ft) (Pekarek, 1977)

Cf **Flathead Sandstone (Middle Cambrian)**—Three distinct units include an upper red to deep red to purple very well indurated sandstone; a middle nonresistant buff to tan to orange, hematite-rich, fine- to medium-grained, well-sorted sandstone; and a lower red to orange, medium- to coarse-grained cross-bedded sandstone and pebble conglomerate. Rare shell hash preserved in thin layers. Thickness is approximately 158 m (520 ft) (Pekarek, 1977)

Archean

Wpg **Pegmatite intrusions (Neoarchean)**—Quartz- and feldspar-dominated pegmatite veins, dikes, and pods intrude the UT Creek Formation on Black Mountain; they both cross-cut and run parallel to foliation, layering, and structure. Some (probably older) pegmatites display evidence of shearing and metamorphism. Width varies from veins less than 2.5 cm (1 in) to large mappable dikes approximately 3 m (10 ft) across. Pegmatite pods associated with prospect pits can be up to 50 m (160 ft) in diameter and locally contain large spodumene, tourmaline, and hornblende crystals

Wmsh **Middle Sage Hen quartz diorite (Neoarchean)**—Fine- to medium-grained, foliated quartz diorite located northwest of Black Mountain; fine-grained mafic enclaves are common. Xenoliths of the UT Creek schist are also present (Langstaff, 1995)

Wesh **East Sage Hen granite (Neoarchean)**—Medium- to coarse-grained, weakly foliated, potassium feldspar-quartz-biotite granite exposed south of Black Mountain; weathers to pink-orange bulbous outcrops with mappable xenoliths of the UT Creek Formation. Dated by Langstaff (1995) to have a minimum crystallization U-Pb age of 2,622 ± 7 Ma, although a maximum is projected at 2,650 Ma

Wfr **French Rocks tonalite (Neoarchean)**—Medium- to coarse-grained, foliated, reddish-brown tonalite to granodiorite containing large hornblende crystals and minor biotite. Forms resistant ridges along Rattlesnake Hills anticline axis. Weathers to brown colored soil. U-Pb zircon geochronology yields 2,655 ± 3 Ma

UT Creek Formation (Neoarchean)

Wutg **Metagraywacke**—Fine- to medium-grained, brownish-red to black, biotite-quartz-plagioclase schist and metaturbidite (Langstaff, 1995); highly foliated. Weathered outcrops have a gravestone appearance. Exposed on north side of Black Mountain. Langstaff (1995) indicates a conformable lower contact with the Asbell metabasalt

Wuta **Asbell metabasalt**—Dark-brown to black, very fine to fine-grained, massive amphibolite tholeiitic metabasalt; pillow structures reported (Hausel, 1996). Comprises majority of central and south Black Mountain

Vbs **Barlow Springs Formation (Mesoarchean)**—Felsic metasedimentary sequence of red to green quartzite with fuchsite, brown to silver metapelite, metabasalt, amphibolite gneiss, and rusty meta-ironstone. Sedimentary structures are rare, but locally observable. Langstaff (1995) reported a detrital zircon age of 3,300 Ma from the quartzite. Metadacites in the upper part dated at 2,856 ± 55 Ma Langstaff (1995) and 2,864 ± 7.8 Ma (Fruchey, 2002)

REFERENCES

Bickford, F.E., 1977, Petrology and structure of the Barlow Gap area, Wyoming: Laramie, University of Wyoming, M.S. thesis, 76 p., scale 1:24,000.

Bogrett, J.W., 1951, Geology of the northwestern end of the Rattlesnake Hills, Natrona County, Wyoming: Laramie, University of Wyoming, M.A. thesis, 70 p., 3 pls., scale 1:24,000.

Burk, C.A., 1956, Subsurface stratigraphy of the pre-Niobrara formations in the Wind River Basin, central Wyoming, *in* Wyoming stratigraphy—Subsurface stratigraphy of the pre-Niobrara formations in Wyoming: Wyoming Geological Association, p. 23–34.

Cola, E.C., and Sutherland, W.M., 2014, Preliminary geologic map of the Mc Intosh Meadows quadrangle, Fremont and Natrona Counties, Wyoming: Wyoming State Geological Survey Open File Report 14-2, 39 p., scale 1:24,000.

Fruchey, B.L., 2002, Archean supracrustal sequences of contrasting origin—The Archean history of the Barlow Gap area, northern Granite Mountains, Wyoming: Laramie, University of Wyoming, M.S. thesis, 178 p., 2 pls., scales 1:3,000 and 1:24,000.

Grace, R.L.B., Chamberlain, K.R., Frost, B.R., and Frost, C.D., 2006, Tectonic histories of the Paleo- to Mesoarchean Sacawee block and Neoarchean Oregon Trail structural belt of the south-central Wyoming Province: Canadian Journal of Earth Sciences, v. 43, no. 10, p. 1445–1466.

Hausel, W.D., 1996, Geology and gold mineralization of the Rattlesnake Hills, Granite Mountains, Wyoming: Wyoming State Geological Survey Report of Investigations 52, 28 p., scale 1:24,000.

Hoch, A.R., 1991, Petrological and geochemical evolution of the Rattlesnake Hills alkaline-intrusive complex, Natrona County, Wyoming: Laramie, University of Wyoming, M.S. thesis, 127 p.

Keefer, W.R., 1965, Stratigraphy and geologic history of the uppermost Cretaceous, Paleocene, and lower Eocene rocks in the Wind River Basin, Wyoming: U.S. Geological Survey Professional Paper 495-A, 77 p., 4 pls., scale ca. 1:380,000.

Keefer, W.R., and Rich, E.I., 1957, Stratigraphy of the Cody Shale and younger Cretaceous and Paleocene rocks in the western and southern parts of the Wind River Basin, Wyoming: Wyoming Geological Association, 12th annual field conference, Guidebook, p. 71–78.

Keefer, W.R., and Van Lieu, J.A., 1966, Paleozoic formations in the Wind River Basin, Wyoming: U.S. Geological Survey Professional Paper 495-B, 60 p., 6 pls., scale ca. 1:500,000.

Langstaff, G.D., 1995, Archean geology of the Granite Mountains: Golden, Colorado School of Mines, Ph.D. dissertation, 671 p., 9 pls., scale 1:24,000.

Love, J.D., 1970, Cenozoic geology of the Granite Mountains area, central Wyoming: U.S. Geological Survey Professional Paper 495-C, 154 p., 10 pls., scale 1:125,000.

Love, J.D., Christiansen, A.C., Earle, J.L., and Jones, R.W., 1979, Preliminary geologic map of the Casper 1° x 2° quadrangle, central Wyoming: U.S. Geological Survey Open File Report 79-961, scale 1:250,000.

Paull, R.A., and Paull, R.K., 1990, Persistent myth about the Lower Triassic Little Medicine Member of the Goose Egg Formation and the Lower Triassic Dinwoody Formation, central Wyoming: Wyoming Geological Association, 41st annual field conference, Guidebook, p. 57–68.

Pekarek, A.H., 1977, Structural geology and volcanic petrology of the Rattlesnake Hills, Wyoming: Wyoming Geological Association Earth Science Bulletin, v. 10, no. 4, p. 3–30.

Pekarek, A.H., 1978, Stratigraphy and structural geology of the Rattlesnake Hills, Wyoming: Wyoming Geological Association, 30th annual field conference, Guidebook, p. 239–253.

Pekarek, A.H., Marvin, R.F., and Mehnert, H.H., 1974, K-Ar ages of the volcanics in the Rattlesnake Hills, central Wyoming: Geology, v. 2, no. 6, p. 283–285.

Roth, K.W., 1955, Stratigraphy of pre-Frontier Cretaceous rocks in Rattlesnake Hills, Natrona County, Wyoming: Laramie, University of Wyoming, M.A. thesis, 102 p., 3 pls.

Sutherland, W.M., and Hausel, W.D., 2003, Geologic map of the Rattlesnake Hills 30' x 60' quadrangle, Fremont and Natrona Counties, Wyoming: Wyoming State Geological Survey Map Series 61, scale 1:100,000.

Sutherland, W.M., and Hausel, W.D., 2005, Geologic map of the Barlow Gap quadrangle, Natrona County, Wyoming: Wyoming State Geological Survey Map Series 67, scale 1:24,000.

Sutherland, W.M., and Worman, B.N., 2013, Preliminary geologic map of the Blackjack Ranch quadrangle, Natrona County, Wyoming: Wyoming State Geological Survey Open File Report 13-3, 24 p., scale 1:24,000.

Toner, R.N., Lynds, R.M., Freye, A.M., and Sutherland, W.M., 2016, Preliminary geologic map of the Ervay Basin quadrangle, Natrona County, Wyoming: Wyoming State Geological Survey Open File Report 16-3, scale 1:24,000.

Van Houten, F.B., 1955, Volcanic-rich middle and upper Eocene sedimentary rocks northwest of Rattlesnake Hills central Wyoming: U.S. Geological Survey Professional Paper 274-A, 14 p.

Van Houten, F.B., 1964, Tertiary geology of the Beaver Rim area Fremont and Natrona Counties, Wyoming: U.S. Geological Survey Bulletin 1164, 99 p., 8 pls., scale 1:62,500.

Van Houten, F.B., and Weitz, J.L., 1956, Geologic map of the eastern Beaver Divide-Gas Hills area, Fremont and Natrona Counties, Wyoming: U.S. Geological Survey Oil and Gas Investigation Map 180, scale 1:63,360.

Wroble, J.L., 1953, Stratigraphy and sedimentation of the Popo Agie, Nugget, and Sundance Formations in central Wyoming: Laramie, University of Wyoming, M.A. thesis, 151 p., 8 pls.

Zeller, H.D., 1957, The Gas Hills uranium district and some probable controls for ore deposition: Wyoming Geological Association, 12th annual field conference, Guidebook, p. 156–160, scale ca. 1:80,000.

Base map from U.S. Geological Survey 1:24,000-scale topographic map of the Ervay Basin SW, Wyoming Quadrangle, 1952, photorevised 1984

Base hillshade derived from United States Elevation Data (NED), 10-meter Digital Elevation Model (DEM), 2009; azimuth 315°, sun angle 45°, vertical exaggeration 2.0

Projection: Universal Transverse Mercator (UTM), zone 13
North American Datum of 1927 (NAD 27)
1,000-meter grid ticks: UTM, zone 13
10,000-foot grid ticks: Wyoming State Plane Coordinate System, east central zone

Wyoming State Geological Survey
P.O. Box 1347 - Laramie, WY 82073-1347
Phone: 307-766-2286 - Fax: 307-766-2605
Email: wsgs-info@wyo.gov

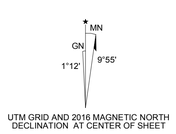

UTM GRID AND 2016 MAGNETIC NORTH DECLINATION AT CENTER OF SHEET

SCALE 1:24,000

1 0.5 0 1 Mile
1,000 0 1,000 2,000 3,000 4,000 5,000 6,000 7,000 Feet
1 0.5 0 1 Kilometer

CONTOUR INTERVAL 20 FEET
NATIONAL GEODETIC VERTICAL DATUM OF 1929

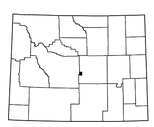

WYOMING QUADRANGLE LOCATION

Digital cartography by Ranie M. Lynds, Amy M. Freye, Rachel N. Toner, and Andrea M. Loveland

Map edited by Suzanne C. Luhr

Prepared in cooperation with and research supported by the U.S. Geological Survey, National Cooperative Geologic Mapping Program, under USGS award number G15AC00514. The views and conclusions contained in this document are those of the authors and should not be interpreted as necessarily representing the official policies, either expressed or implied, of the U.S. Government.

PRELIMINARY GEOLOGIC MAP OF THE ERVAY BASIN SW QUADRANGLE, NATRONA COUNTY, WYOMING

by

Ranie M. Lynds, Rachel N. Toner, Amy M. Freye, Wayne M. Sutherland, and Andrea M. Loveland

2016

DISCLAIMERS

Users of this map are cautioned against using the data at scales different from those at which the map was compiled. Using these data at a larger scale will not provide greater accuracy and is a misuse of the data.

The Wyoming State Geological Survey (WSGS) and the State of Wyoming make no representation or warranty, expressed or implied, regarding the use, accuracy, or completeness of the data presented herein, or of a map printed from these data. The act of distribution shall not constitute such a warranty. The WSGS does not guarantee the digital data or any map printed from the data to be free of errors or inaccuracies.

The WSGS and the State of Wyoming disclaim any responsibility or liability for interpretations made from these digital data or from any map printed from these digital data, and for any decisions based on the digital data or printed maps. The WSGS and the State of Wyoming retain and do not waive sovereign immunity.

The use of or reference to trademarks, trade names, or other product or company names in this publication is for descriptive or informational purposes only, or is pursuant to licensing agreements between the WSGS or State of Wyoming and software or hardware developers/vendors, and does not imply endorsement of those products by the WSGS or the State of Wyoming.

NOTICE TO USERS OF INFORMATION FROM THE WYOMING STATE GEOLOGICAL SURVEY

The WSGS encourages the fair use of its material. We request that credit be expressly given to the "Wyoming State Geological Survey" when citing information from this publication. Please contact the WSGS at 307-766-2286, ext. 224, or by email at wsgs-info@wyo.gov if you have questions about citing materials, preparing acknowledgments, or extensive use of this material. We appreciate your cooperation.

Individuals with disabilities who require an alternative form of this publication should contact the WSGS. For the TTY relay operator call 800-877-9975.

For more information about the WSGS or to order publications and maps, go to www.wsgs. wyo.gov, call 307-766-2286, ext. 224, or email wsgs-info@wyo.gov.

NOTICE FOR OPEN FILE REPORTS PUBLISHED BY THE WSGS

This WSGS Open File Report has not been technically reviewed or edited for conformity with WSGS standards or Federal Geographic Data Committee digital cartographic standards. Open File Reports are preliminary and usually require additional fieldwork and/or compilation and analysis; they are meant to be a first release of information for public comment and review. The WSGS welcomes any comments, suggestions, and contributions from users of the information.

WYOMING STATE GEOLOGICAL SURVEY

P.O. BOX 1347, LARAMIE, WY 82073
307-766-2286 • 307-766-2605 (fax)
wsgs-info@wyo.gov • www.wsgs.wyo.gov
Director & State Geologist
Thomas A. Drean

Preliminary Geologic Map
of the
Ervay Basin SW Quadrangle
Natrona County, Wyoming

by

Ranie M. Lynds, Rachel N. Toner, Amy M. Freye, Wayne M. Sutherland, and Andrea M. Loveland

Open File Report 2016-4
Laramie, Wyoming
2016

Prepared in cooperation with and research supported by the U.S. Geological Survey, National Cooperative Geologic Mapping Program, under USGS award number G15AC00514. The views and conclusions contained in this document are those of the authors and should not be interpreted as necessarily representing the official policies, either expressed or implied, of the U.S. Government.

This report is preliminary and has not been reviewed for conformity with Wyoming State Geological Survey editorial standards or with the North American Stratigraphic Code.

CONTENTS

INTRODUCTION

This mapping project was selected to better understand how structural processes in the area have affected local and regional geologic features and contributed to the formation of the Rattlesnake Hills, Granite Mountains, and Wind River Basin. Study of the deformation processes helps to explain current oil and gas production and may possibly identify future development trends. New mapping also provides a base for interpretation related to other possible strategic mineral resources, including uranium, rare earth elements, and other economic minerals in the basin.

A secondary goal was to identify the spatial and temporal relationships of coeval Tertiary volcanic flows and the Wagon Bed Formation. Radiometric dating and geochemical analyses conducted for this project helps clarify the history and extent of Rattlesnake Hills volcanism. Although multiple radiometric ages have been acquired in the general area (Pekarek and others, 1974; Peterman and Hildreth, 1978; Langstaff, 1995; Fruchey, 2002), no prior geochronology currently exists from the study area.

Portions of the Ervay Basin SW 7.5' quadrangle have been mapped at various scales by Bogrett (1951), Van Houten and Weitz (1956), Zeller and others (1956), Van Houten (1964), Pekarek (1974, 1978), and Langstaff (1995). Nearby Rattlesnake Hills volcanics were also previously mapped by Carey (1954, 1959). No detailed 1:24,000-scale map of the Ervay Basin SW quadrangle has ever been published.

Mapping was conducted through on-the-ground examination and measurement of rock units, aerial imagery interpretation, and compilation of previous mapping and written reports. Initial mapping of the quadrangle began with aerial photographic interpretation and minor field spot checks by Wayne M. Sutherland during 2001 and 2002, which was incorporated into the 1:100,000-scale Rattlesnake Hills 30' x 60' quadrangle (Sutherland and Hausel, 2003). The principal investigators made an initial visit to the Ervay Basin SW quadrangle in September, 2015, to become familiar with the area, access routes, and basic geology. Field work was conducted from May through August 2016.

This project was completed in cooperation with the U.S. Geological Survey 2015 StateMap grant award G15AC00514 to the Wyoming State Geological Survey. This map is part of a two-map project that includes both the Ervay Basin (Toner and others, 2016) and Ervay Basin SW 1:24,000-scale quadrangles.

We wish to acknowledge the Clear Creek Cattle Co., Coffman Ranch Co., Herbst Lazy TY Cattle Co., Circle Bar Ranch, and LHS Split Rock for access to their private lands to complete this map.

LOCATION AND GEOLOGIC SETTING

The Ervay Basin SW 1:24,000-scale quadrangle in central Wyoming is approximately 85 km (53 mi) west-southwest of Casper, 80 air km (50 mi) east-southeast of Riverton, and 47 km (29 mi) northeast of Jeffrey City. Elevations range from 2,450 m (8,040 ft) above sea level on Black Mountain in the southwestern corner of the quadrangle to less than 2,090 m (6,860 ft) at the northwestern corner of the quadrangle. The climate within the study area is high desert; grasses and sage represent the majority of vegetation. Isolated pine and juniper trees are found at the higher elevations, with wetter environment vegetation growing along northwest-flowing Deer and East Canyon Creeks and the southwest-flowing Middle Fork Sage Hen Creek.

Access to the area is from the graded Dry Creek Road (Natrona County 321), which leaves Wyoming State Highway 220 about 7.2 km (4.5 mi) northeast of Independence Rock and leads northwesterly about 36.2 km (22.5 mi) to the east-central portion of the quadrangle. Several side roads of varying conditions branch off the Dry Creek Road, providing general access to much of the study area.

The Ervay Basin SW 1:24,000-scale geologic map is located immediately north of the Granite Mountains along the western side of the complexly folded and faulted northwest-plunging Rattlesnake Hills anticline. Laramide deformation and uplift is evident in the Archean tonalitic gneiss exposed in the core of the Rattlesnake Hills anticline. Further evidence of Laramide processes can be seen in Archean supracrustal assemblages of granite, schist, metabasalt, and diorite that crop out near and on Black Mountain.

Paleozoic and Mesozoic units form the limbs of the Rattlesnake Hills anticline. A small exposure of these same formations also occurs in the west-central portion of the quadrangle near a reclaimed uranium mine. These exposures are likely associated with and may be an extension of the Dutton anticline further west and north of the map area.

Tertiary rock unit exposures within the study area are dominated by the Eocene Wind River Formation to the north and the Eocene Wagon Bed Formation in the southern half of the quadrangle. Tertiary Wind River and Wagon Bed Formations conceal the southern portion of the Rattlesnake Hills anticline's limbs. Wind River, Wagon Bed, White River, and Split Rock Formations overlie the eastern edge of the Beaver Divide escarpment and form valley fill deposits. The Oligocene White River Formation crops out along Beaver Rim as an isolated disconformable channel fill on the western side of the quadrangle.

Eocene volcanic flows are also present in the south-central portion of the map area and are locally interbedded with the Wagon Bed Formation. Uranium prospects and reclaimed surface uranium mines within the Wind River Formation are prominent along the western edge of the quadrangle.

STRUCTURE

The northwest-plunging Rattlesnake Hills anticline is the eastern-most fold in a series of anticlines that comprise the southern flank of the Wind River Basin. Laramide deformation and uplift are evident in the anticline's exposed Precambrian core and in the complex folding and faulting of the Paleozoic, Mesozoic, and some Cenozoic units that dominate the limbs and nose of the anticline.

Primary folding and faulting occurred during the Laramide, with deformation continuing until at least the early Eocene. Fracture and fault data from the central and northern Wind River Basin suggest Laramide-age compression (maximum compressive stress oriented N66°E), followed by extension and relaxation with minimum compressive stresses oriented N44°E and N7°E, respectively (Thompson, 2010).

ECONOMICS

The active Raderville oil field is situated within the northern axis of the Rattlesnake Hills anticline, on the adjacent Ervay Basin quadrangle (Toner and others, 2016). Oil and gas is produced north of the map area from a combination of stratigraphic and structural traps involving many of the same formations exposed in the core of the anticline. The Cretaceous and Tertiary outcrops in the project area are an excellent analog to subsurface oil and gas reservoirs and source rocks.

Historic uranium prospect pits found in outcrops of the Wind River and Wagon Bed Formations and reclaimed surface mines in the western part of the quadrangle attest to past uranium mining and indicate potential for uranium resources in the area. The Wind River Formation in the Gas Hills, a few miles west of the quadrangle, contains significant concentrations of ore grade uranium deposits. The Gas Hills area produced more than 100 million pounds of U_3O_8 concentrate (yellowcake) since mining began in the 1950s (R.W. Gregory, oral commun., 2016).

Occurrences south and east of the Ervay Basin SW quadrangle suggest some potential for gold and associated metals, and gemstones (Hausel, 1996; Hausel and Sutherland, 2000; Koehler, 2012; Sutherland and Worman, 2013). However, no anomalous concentrations of these mineral resources were found while mapping the quadrangle. Exploration in the last several years for both gold and rare earth elements by companies and individuals has focused on the Eocene volcanics and related alteration zones within Precambrian rocks.

SAMPLES

Although numerous samples were collected during fieldwork, a total of seven samples were analyzed for U-Pb geochronology, four of which were also analyzed for whole rock and trace geochemistry, and one additional sample was analyzed for geochemistry alone. These samples are noted on the map plate. Table 1 lists the analyses conducted per sample.

Table 1. List of samples, locations, and type of analyses. Results for samples followed by an asterisk (*) are expected in early 2017 and are not part of this report. Latitude and longitude reported in WGS84.

Sample	Formation	Latitude	Longitude	Geochemistry	Geochronology
20150925RL-01	Tv	42.75006	-107.39787	X	
20150925RL-03	Twb	42.75500	-107.40821	X	X
20150925RL-04	Tv	42.78048	-107.39989	X	X
20150925RL-05	Twb	42.79355	-107.39159	X	X
20150925RL-07	Wfr	42.83602	-107.37679	X	X
20160801RT-01*	Twb	42.76683	-107.45128		X
20160801RT-02*	Twr	42.78377	-107.48476		X
20160802RT-01*	Tv	42.75500	-107.39187		X

Sample results are reported in Appendix 1, 2, and 2, and are also available from the Wyoming State Geological Survey's Wyoming Database of Geology (Wyo-DOG).

REFERENCES

Barth, A.P., Wooden, J.L., Mueller, P. A., and Economos, R. C., 2016, Granite provenance and intrusion in arcs—Evidence from diverse zircon types in Big Bear Lake Intrusive Suite, USA: Lithos, v. 246, p. 261–278.

Bogrett, J.W., 1951, Geology of the northwestern end of the Rattlesnake Hills, Natrona County, Wyoming: Laramie, University of Wyoming, M.A. thesis, 70 p., 3 pls., scale 1:24,000.

Carey, B.D., 1954, Geologic map and structure sections of the Rattlesnake Hills Tertiary volcanic field: Wyoming Geological Association 9th annual field conference, Guidebook, p. 32–34.

Carey, B.D., 1959, Geology of the Rattlesnake Hills Tertiary volcanic field, Natrona County, Wyoming: Laramie, University of Wyoming, Ph.D. dissertation, 247 p., 36 pls.

Chamberlain, K.R., Frost, C.D., and Frost, B.R., 2003, Early Archean to Mesoproterozoic evolution of the Wyoming Province—Archean origins to modern lithospheric architecture: Canadian Journal of Earth Sciences, v. 40, no. 10, p. 1357–1374.

Chamberlain, K.R., Kilian, Taylor, Evans, D.A.D., and Bleeker, Wouter, 2015, Late Archean to Proterozoic reconstructions of Wyoming and Superior cratons: Geological Society of America Abstracts with Programs, v. 47, no. 7, p. 447.

Koehler, 2012, Evolving Gold Corp. national instrument 43-101 technical report on the Rattlesnake Hills project, Natrona County, Wyoming, USA: Evolving Gold Corporation, accessed June 2016, at http://www.evolvinggold.com/i/pdf/Rattlesnake_43-101_2012final6Feb12.pdf.

Frost, B.R., Chamberlain, K.R., and Schumacher, J.C., 2000, Sphene (titanite)—Phase relations and role as a geochronometer: Chemical Geology, v. 172, p. 131–148.

Frost, C.D., Frost, B.R., Kirkwood, Robert, and Chamberlain, K.R., 2006a, The tonalite-trondhjemite-granodiorite (TTG) to granodiorite-granite (GG) transition in the Neoarchean plutonic rocks of the central Wyoming province: Canadian Journal of Earth Sciences, v. 43, no. 10, p. 1419–1444.

Frost, B.R., Frost, C.D., Cornia, Mary, Chamberlain, K.R., and Kirkwood, Robert, 2006b, The Teton-Wind River domain—a 2.68-2.67 Ga active margin in the western Wyoming Province: Canadian Journal of Earth Sciences, v. 43, no. 10, p. 1489–1510.

Frost, C.D., Fruchey, B.L., Chamberlain, K.R., and Frost, B.R., 2006c, Archean crustal growth by lateral accretion of juvenile supracrustal belts in the south-central Wyoming province: Canadian Journal of Earth Sciences, v. 43, no. 10, p. 1533–1555.

Fruchey, B.L., 2002, Archean supracrustal sequences of contrasting origin—the Archean history of the Barlow Gap area, northern Granite Mountains, Wyoming: Laramie, University of Wyoming, M.S. thesis, 178 p., scale 1:3,000 and 1:24,000.

Grace, R.L.B., Chamberlain, K.R., Frost, B.R., and Frost, C.D., 2006, Tectonic histories of the Paleo- to Mesoarchean Sacawee block and Neoarchean Oregon Trail structural belt of the south-central Wyoming Province: Canadian Journal of Earth Sciences, v. 43, no. 10, p. 1445–1466.

Hanchar, J.M., and Miller, C.F., 1993, Zircon zonation patterns as revealed by cathodoluminescence and backscattered electron images—Implications for interpretation of complex crustal histories: Chemical Geology, v. 110, p. 1–13.

Hausel, W.D., 1996, Geology and gold mineralization of the Rattlesnake Hills, Granite Mountains, Wyoming: Wyoming State Geological Survey Report of Investigations 52, 28 p., scale 1:24,000.

Hausel, W.D., and Sutherland, W.M., 2000, Gemstones and other unique minerals and rocks of Wyoming—A field guide for collectors: Wyoming State Geological Survey Bulletin 71, 268 p.

Kilian, T.M., Bleeker, Wouter, Chamberlain, Kevin, Evans, D.A.D., and Cousens, Brian, 2015, Palaeomagnetism, geochronology and geochemistry of the Palaeoproterozoic Rabbit Creek and Powder River dyke swarms—Implications for Wyoming in supercraton Superia, *in* Li, Z.X., Evans, D.A.D., and Murphy, J.B., Supercontinent cycles through Earth history: Geological Society, London, Special Publications, 424, p. 15–45.

Krogh, T.E., 1973, A low-contamination method for hydrothermal decomposition of zircon and extraction of U and Pb for isotopic age determinations: Geochimica et Cosmochimica Acta, v. 37, p. 485–494.

Langstaff, G.D., 1995, Archean geology of the Granite Mountains: Golden, Colorado School of Mines, Ph.D. dissertation, 671 p., scale 1:24,000.

Ludwig, K.R., l988, PBDAT for MS-DOS, a computer program for IBM-PC compatibles for processing raw Pb-U-Th isotope data, version 1.24: U.S. Geological Survey Open-File Report 88-542, 32 p.

Ludwig, K.R., l991, ISOPLOT for MS-DOS, a plotting and regression program for radiogenic-isotope data, for IBM-PC compatible computers, version 2.75: U.S. Geological Survey Open-File Report 91-445, 45 p.

Ludwig, K.R., 1998, On the treatment of concordant uranium-lead ages: Geochimica et Cosmochimica Acta, v. 62, no. 4, p. 665–676.

Mattinson, J.M., 2005, Zircon U-Pb chemical abrasion ("CA-TIMS") method—Combined annealing and multi-step partial dissolution analysis for improved precision and accuracy of zircon ages: Chemical Geology, v. 220, p. 47–66.

Parker, G., Chamberlain, K.R., and Siddoway, C., 2015, The Powder River Pass shear zone—Roots of an Archean foreland thrust fault?: Geological Society of America Abstracts with Programs, v. 47, no. 6, p.39.

Parrish, R.R., Roddick, J.C., Loveridge, W.D., and Sullivan, R.D., l987, Uranium-lead analytical techniques at the geochronology laboratory, Geological Survey of Canada, *in* Radiogenic age and isotopic studies, Report 1: Ottawa, Geological Survey of Canada Paper 87-2, p. 3–7.

Pekarek, A.H., 1974, Structural geology and volcanic petrology of the Rattlesnake Hills, Wyoming: Laramie, University of Wyoming, Ph.D. dissertation, 111 p., scale 1:50,000.

Pekarek, A.H., 1978, Stratigraphy and structural geology of the Rattlesnake Hills, Wyoming: Wyoming Geological Association, 30th annual field conference, Guidebook, p. 239–253.

Pekarek, A.H., Marvin, R.F., and Mehnert, H.H., 1974, K-Ar ages of the volcanics in the Rattlesnake Hills, central Wyoming: Geology, v. 2, p. 283–285.

Peterman, Z.E., and Hildreth, R.A., 1978, Reconnaissance geology and geochronology of the Precambrian of the Granite Mountains, Wyoming: U.S. Geological Survey Professional Paper 1055, 22 p.

Stacey, J.S., and Kramers, J.D., 1975, Approximation of terrestrial lead isotope evolution by a two-stage model: Earth and Planetary Science Letters, v. 26, p. 207–221.

Steiger, R.H., and Jäger, E., 1977, Subcommission on geochronology—Convention on the use of decay constants in geo- and cosmochronology: Earth and Planetary Science Letters, v. 36, p. 359–362.

Sutherland, W.M., and Hausel, W.D., 2003, Geologic Map of the Rattlesnake Hills 30' x 60' quadrangle, Fremont and Natrona Counties, Wyoming: Wyoming State Geological Survey Map Series 61, 28 p., scale 1:100,000.

Sutherland, W.M., and Worman, B.N., 2013, Preliminary geologic map of the Blackjack Ranch quadrangle, Natrona County, Wyoming: Wyoming State Geological Survey Open File Report 13-3, 24 p., scale 1:24,000.

Thompson, R.C., 2010, Two-stage development of the Wind River Basin, Wyoming—Laramide shortening followed by post-Laramide regional extension, localized backsliding, and arch collapse: Fort Collins, Colorado State University, M.S. thesis, 118 p.

Tilton, G.R., 1973, Isotopic lead ages of chondritic meteorites: Earth and Planetary Science Letters, v. 19, no.3, p. 321–329.

Toner, R.N., Lynds, R.M., Freye, A.M., Sutherland, W.M., 2016, Preliminary geologic map of the Ervay Basin quadrangle, Natrona County, Wyoming: Wyoming State Geological Survey Open File Report 16-3, scale 1:24,000.

Van Houten, F.B., 1964, Tertiary geology of the Beaver Rim area Fremont and Natrona Counties, Wyoming: U.S. Geological Survey Bulletin 1164, 99 p., 8 pls., scale 1:62,500.

Van Houton, F.B., and Weitz, J.L., 1956, Geologic map of the eastern Beaver Divide-Gas Hills area, Fremont and Natrona Counties, Wyoming: U.S. Geological Survey Oil and Gas Investigations Map 180, scale 1:63,360.

Verts, L.A., Chamberlain, K.R., and Frost, C.D., 1996, U-Pb sphene dating of metamorphism—the importance of sphene growth in the contact aureole of the Red Mountain Pluton, Laramie Mountains, Wyoming: Contributions to Mineralology and Petrolology, v. 125, p. 186–199.

Zeller, H.D., Soister, P.E., and Hyden, H.J., 1956, Preliminary geologic map of the Gas Hills Uranium District, Fremont and Natrona Counties, Wyoming: U.S. Geological Survey Mineral Investigations Field Studies Map MF-83, scale 1:31,680.

APPENDIX 1: GEOCHEMICAL ANALYSES

Table A1-1. Geochemical analyses, including whole rock chemistry, trace elements, rare earth elements, and gold, were completed by ALS Chemex of Reno, Nevada. LOI is loss on ignition. Full report available from the Wyo-DOG database.

	SiO_2	Al_2O_3	Fe2O3	CaO	MgO	Na_2O	K_2O	Cr_2O_3	TiO_2	MnO	P_2O_5	SrO	BaO	C
Sample	%	%	%	%	%	%	%	%	%	%	%	%	%	%
20150925RL-01	68.5	14.5	3.72	3.03	0.96	4.26	2.57	<0.01	0.36	0.08	0.2	0.13	0.1	0.04
20150925RL-03	60.3	16.9	5.01	4.36	1.76	4.59	2.3	<0.01	0.5	0.12	0.38	0.18	0.08	0.07
20150925RL-04	64.7	17.1	4.17	3.72	0.98	5.18	2.98	<0.01	0.41	0.1	0.27	0.17	0.09	0.05
20150925RL-05	69.4	13.55	2.17	1.33	0.53	1.12	2	<0.01	0.29	0.02	0.01	0.02	0.09	0.16
20150925RL-07	62.4	16.05	5.33	5.24	2.82	4.52	1.79	0.01	0.55	0.08	0.28	0.09	0.09	0.23

	S	Ba	Ce	Cr	Cs	Dy	Er	Eu	Ga	Gd	Ge	Hf	Ho	La
Sample	%	ppm	ppm	ppm	ppm	ppm	ppm	ppm	ppm	ppm	ppm	ppm	ppm	ppm
20150925RL-01	<0.01	869	76.2	20	4.25	4.1	2.3	1.59	18.7	5.13	<5	4.6	0.81	40.7
20150925RL-03	0.01	679	80.5	10	2.4	4.39	2.4	1.98	21.6	6.18	<5	6	0.84	42.4
20150925RL-04	<0.01	797	74.2	10	1.56	4	2.39	1.85	20.8	5.22	<5	5.3	0.8	41.1
20150925RL-05	0.05	814	69.1	10	4.94	2.62	1.41	0.65	16.9	3.18	<5	7.7	0.52	40.5
20150925RL-07	<0.01	795	101.5	80	0.63	2.43	1.05	1.54	19.4	4.32	<5	3.7	0.39	51.2

	Lu	Nb	Nd	Pr	Rb	Sm	Sn	Sr	Ta	Tb	Th	Tm	U	V
Sample	ppm	ppm	ppm	ppm	ppm	ppm	ppm	ppm	ppm	ppm	ppm	ppm	ppm	ppm
20150925RL-01	0.34	17.2	32.2	8.23	64.4	5.89	1	1060	1	0.75	9.17	0.37	2.62	56
20150925RL-03	0.34	18	35.7	9.29	66.4	6.61	1	1475	0.9	0.82	8.58	0.34	3.06	79
20150925RL-04	0.34	19.8	32.7	8.41	62.3	6.01	1	1355	1.1	0.72	8.8	0.36	2.9	79
20150925RL-05	0.21	22.7	25.8	7.55	97.9	4.38	3	186	1.7	0.5	12.2	0.24	3.72	21
20150925RL-07	0.12	3.8	42.8	11.2	34.2	6.57	1	727	0.2	0.52	7.36	0.16	1.22	82

	W	Y	Yb	Zr	As	Bi	Hg	In	Re	Sb	Se	Te	Tl
Sample	ppm	ppm	ppm	ppm	ppm	ppm	ppm	ppm	ppm	ppm	ppm	ppm	ppm
20150925RL-01	1	21.7	2.23	185	1.5	0.2	<0.005	0.017	<0.001	0.17	0.6	<0.01	0.13
20150925RL-03	1	23.3	2.26	243	0.9	0.15	0.006	0.019	<0.001	0.13	0.4	0.01	0.11
20150925RL-04	1	21.6	2.27	211	1.3	0.07	0.005	0.023	<0.001	0.13	0.6	<0.01	0.03
20150925RL-05	2	13.3	1.45	288	1.1	0.14	0.021	0.012	<0.001	0.1	0.5	0.01	0.27
20150925RL-07	<1	10.8	0.9	157	0.5	0.05	0.005	0.01	<0.001	0.08	0.4	<0.01	0.13

	LOI	Total	Ag	Cd	Co	Cu	Li	Mo	Ni	Pb	Sc	Zn
Sample	%	%	ppm	ppm	ppm	ppm	ppm	ppm	ppm	ppm	ppm	ppm
20150925RL-01	1.74	100.15	<0.5	<0.5	5	9	20	<1	7	20	5	64
20150925RL-03	4.09	100.57	<0.5	<0.5	8	41	20	<1	6	20	6	90
20150925RL-04	0.48	100.35	<0.5	<0.5	6	5	20	<1	3	18	5	70
20150925RL-05	11.25	101.78	<0.5	<0.5	2	5	20	1	5	24	4	42
20150925RL-07	1.25	100.5	<0.5	<0.5	16	10	20	<1	45	9	9	70

The samples collected for geochemical analyses are grab samples, which generally do not represent a large or measured volume of material greater than that of the sample itself. Elemental concentrations associated with a grab sample may or may not extend into the outcrop from which the sample was collected. Analyses of these samples can neither confirm nor deny the presence or absence of economic concentrations of various elements.

APPENDIX 2: GEOCHRONOLOGIC EVALUATION OF SAMPLES 20150925RL-03, 20150925RL-04, AND 20150925RL-05

Report by:

Kevin R. Chamberlain, Research Professor, University of Wyoming, July 28, 2016

Introduction

Zircons recovered from these samples ranged from rounded grains, which are likely detrital Precambrian zircons, to euhedral, colorless grains that may represent an ash-fall component (fig. A2-1). Some of the euhedral grains exhibit characteristics that are associated with volcanic origins, such as elongate tips and longitudinal bubble tracks. Figure A2-1 represents the approximate proportions of rounded, detrital grains versus euhedral and ash-type morphologies that were recovered from each sample. Older detrital grains are commonly found in volcanic rocks and were likely entrained either from the country rocks during eruption or from the surface or during deposition. Subpopulations of the euhedral and ash-type zircons were selected for analysis to try to determine the ages of the volcanic components.

Cathodoluminescent (CL) imaging of the selected grains revealed very smooth patterns with single domains within each crystal (fig. A2-2). CL domains typically reflect variations in U concentrations, and zircons from plutonic rocks often display distinct concentric zoning as the uranium concentrations of the magma varies during zircon crystallization (e.g. Hanchar and Miller 1993; Barth and others, 2016). The smooth, simple CL characteristics of the sample zircons reflect a single magma composition during crystallization and are consistent with a volcanic origin for the zircons, with relatively rapid crystallization before eruption.

Samples were dated by laser ablation inductively-coupled plasma mass spectrometric method (LA-ICP-MS). The chief advantage of LA-ICP-MS is that many individual zircons can be analyzed quickly and relatively cheaply. It is an excellent approach for screening zircons to identify multiple age components. The chief disadvantages of LA-ICP are that the individual zircon dates are less precise than by dissolution methods such as chemical abrasion and thermal ionization mass spectrometry (CA-TIMS, 2.0 percent versus 0.2 percent), and it is difficult to measure ^{204}Pb due to interferences from trace mercury (^{204}Hg) in the argon carrier gas. ^{204}Pb is the only non-radiogenic isotope of Pb and is used in CA-TIMS methods to determine and correct for the common Pb component in the analyses. LA-ICP data must be corrected for common Pb by model-dependent, less direct methods.

Two methods for correction of common Pb are used in this report, a total Pb isochron approach and ^{207}Pb-correction method. Both methods assume that the zircons have not lost any Pb and that the measured Pb isotopic compositions are two-component mixtures of radiogenic and common Pb. These assumptions are most appropriate for Phanerozoic-aged zircons, which have relatively minor crystal lattice damage and relatively higher proportions of common Pb than do Precambrian zircons. The total Pb isochron approach uses linear regressions to calculate radiogenic (interpreted as magmatic) and common Pb endmembers from a number of analyses. The ^{207}Pb-correction method can be applied to individual analyses by assuming a common Pb ^{207}Pb/^{206}Pb and calculating the ^{206}Pb/^{238}U date of the concordia intercept on the associated Pb mixing line.

Approximately 100 euhedral grains from each sample were mounted in epoxy, polished to 1/2 depth, and analyzed at the University of California Santa Barbara by Dr. John Cottle. For 20150925RL-03 and -04, there was such a large range in grain sizes that two separate mounts were prepared, one with large grains and one with smaller grains so that polishing would reach the approximate mid-point for each size. Laser spot sizes were approximately 10 microns, and down-hole fractionations were corrected by direct comparison to three standards using the Iolite data reduction program. Concordia intercepts and weighted mean calculations used Isoplot, based on Ludwig (1991).

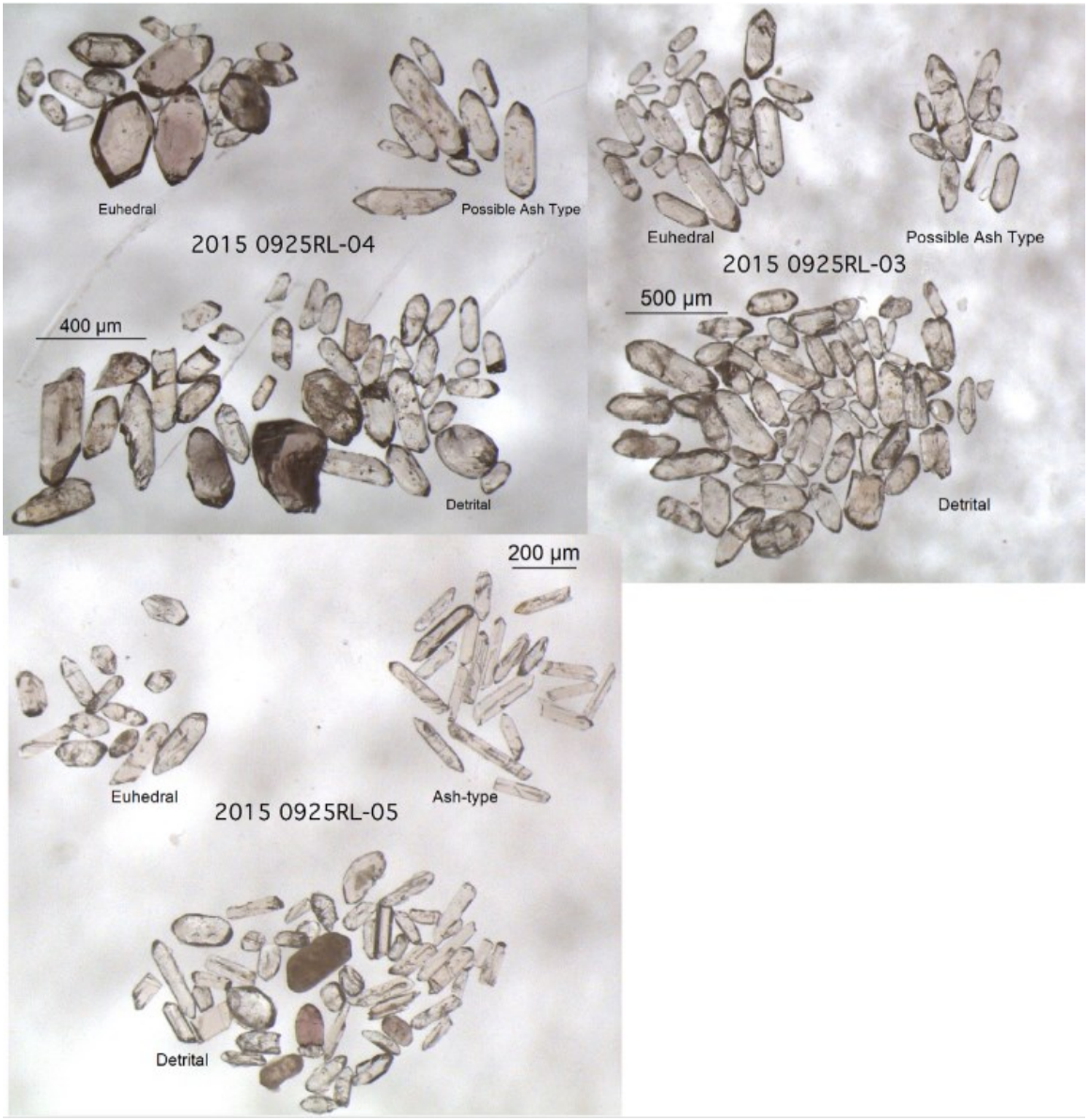

Figure A2-1. Examples of zircons recovered from each volcanic sample. The three groups in each image represent morphologies separated from bulk splits, so the numbers of grains reflect the approximate proportions of each zircon type. Ash-type grains are typically elongate, with longitudinal bubble trails and transverse channels, characteristics that are consistent with crystallization in a low-pressure, gas-rich magma such as the eruptive chamber of a volcano. Ash-type and euhedral subpopulations were selected for age determinations by LA-ICP-MS.

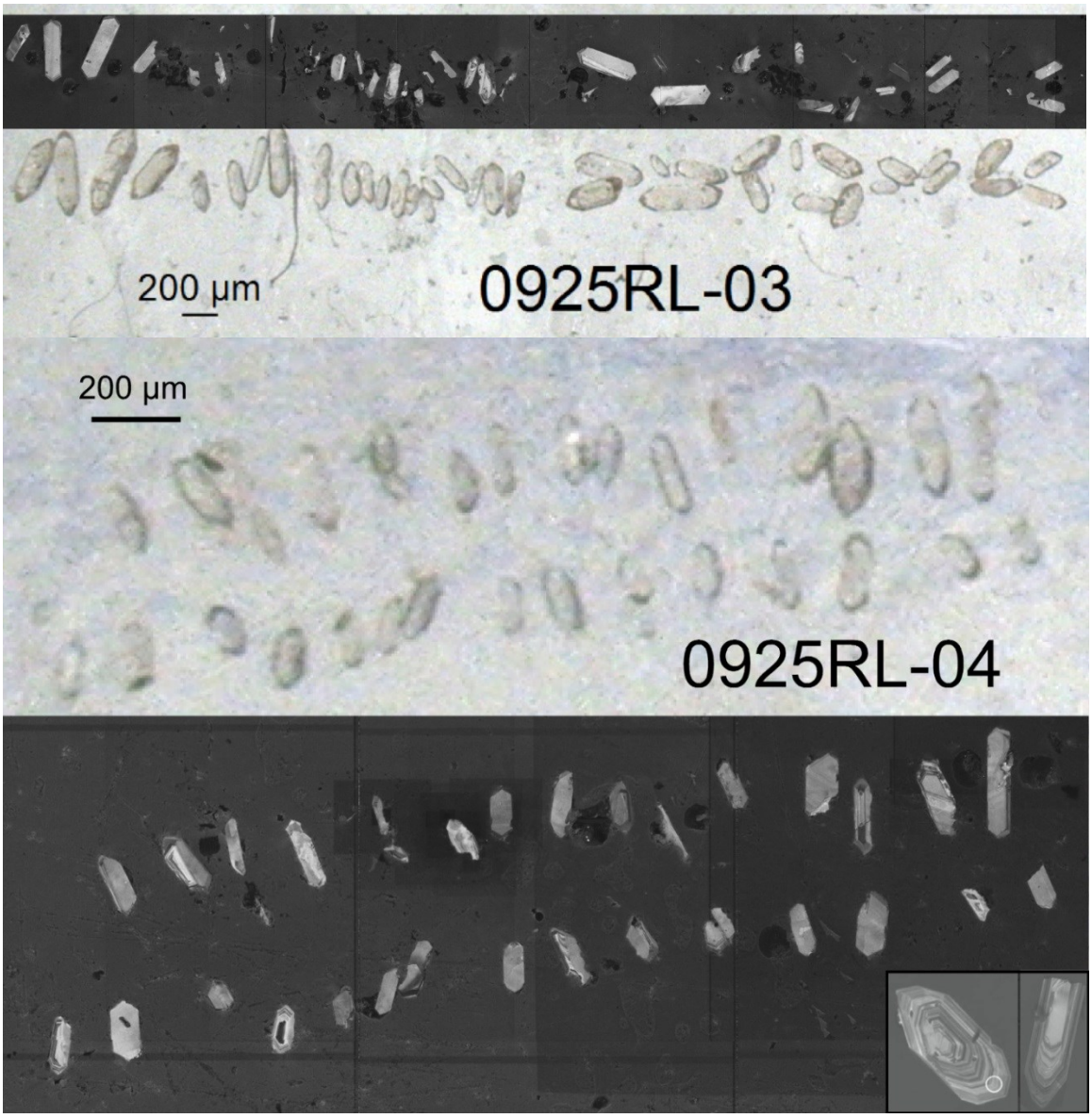

Figure A2-2. Plain light and corresponding cathodoluminescent (dark background) images of zircons from 20150925RL-03 and -04 analyzed by LA-ICP-MS. The upper images (-03) are from the large grain mount, note scale bar; the lower images (-04) are from the mount of smaller zircon grains. The CL patterns from both large and small grains are consistently smooth, with only slight variations, a pattern that supports volcanic origins for these grains. The inset at lower right shows concentric CL zoning that is typical of zircons from plutonic rocks (Barth and others, 2016) in contrast to the smooth patterns from the volcanic rocks.

Results

2015-0925RL-03: 60 LA-ICP spot analyses including both large and small euhedral to ash-type grains yielded a relatively narrow range of ^{207}Pb-corrected ^{206}Pb/^{238}U dates from ca. 44 to 52 Ma (table A2-1). None of the analyzed grains in this sample yielded dates from distinctly detrital sources. Total Pb linear regression of 57 of these young grains yields a lower intercept date of 45.6±0.2 Ma (fig. A2-3), with a fairly reasonable MSWD of 2.0. The favored date for volcanism in this sample comes from the weighted mean ^{207}Pb-corrected ^{206}Pb/^{238}U date of 45.4±0.2 Ma from a subset of the 47 youngest dates (fig. A2-3).

2015-0925RL-04: 46 LA-ICP spot analyses including both large and small euhedral to ash-type grains yielded a relatively narrow range of ^{207}Pb-corrected ^{206}Pb/^{238}U dates from ca. 48 to 43 Ma (table A2-2). Four additional grains yielded ^{207}Pb/ ^{206}Pb dates from 2,579 to 2,657 Ma and are interpreted to reflect detrital dates. The abundance of similar dates from the selected euhedral and ash-type sub-populations indicates that the morphological criteria successfully isolated a dominantly volcanic population. Total Pb linear regression of 45 of these young grains yields a lower intercept date of 45.8±0.4 Ma (fig. A2-4), although the MSWD of 3.9 indicates some excess scatter. The favored date for volcanism in this sample comes from the weighted mean ^{207}Pb-corrected ^{206}Pb/^{238}U date of 45.2±0.2 Ma from a subset of the 26 youngest dates (fig. A2-5).

2015-0925RL-05: 30 LA-ICP spot analyses of euhedral to ash-type grains yielded a relatively narrow range of ^{207}Pb-corrected ^{206}Pb/^{238}U dates from ca. 46 to 52 Ma (table A2-3). None of the analyzed grains in this sample yielded dates from distinctly detrital sources. The favored date for volcanism in this sample comes from the weighted mean ^{207}Pb-corrected ^{206}Pb/^{238}U date of 47.9±0.3 Ma from a subset of the 17 youngest dates (fig. A2-6). Total Pb linear regression of these 17 young grains yields a lower intercept date of 48.0±0.3 Ma (fig. A2-6), with an excellent MSWD of 1.0. This date is within error of the ^{207}Pb-corrected ^{206}Pb/^{238}U weighted mean date.

Based on the uncertainties between these volcanic dates from the study area, the depositional interval between the upper two samples is a maximum of 0.63 Ma at the limits of uncertainty. Differences in volcanic ages between the lower two samples range from a minimum of 1.97 Ma to a maximum of 2.91 Ma (fig. A2-7).

Table A2-1. Sample 150925RL-03, 45.44±0.19 Ma 95 percent confidence, weighted mean ^{207}Pb-corr. ^{206}Pb/^{238}U date (MSWD 1.4), 47/60 spots. Data acquired by laser ablation ICP-MS at UC Santa Barbara, March 2016. All ratios and dates are total Pb, which includes common Pb, except the column labelled 207Pb-corrected. excl. = data excluded from calculated date: r = red ellipses on concordia plots, e = additional excluded from weighted mean calculation, *A = Archean detrital grains.

order	sample name spot#	X	Y	Pb (ppm)	U (ppm)	Th (ppm)	Th/U	207/206	2SE %	207/235	2SE %	206/238	2SE %	Rho	excl.	207/206 Date (Ma)	2 SE abs.	206/238 Date (Ma)	2 SE abs.	207Pb corr'd 206/238 Date (Ma)	2 SE abs.
31	0925RL-03_1	9812	75948	17	366	327	0.88	0.1940	10.4	0.24	11.2	0.00873	4.1	0.4		2700	170	56	2	45.7	2.4
32	0925RL-03_2	9825	75996	15	241	150	0.62	0.2320	16.0	0.316	17.3	0.00944	6.5	0.4		2890	256	61	4	46.5	4.1
33	0925RL-03_3	9873	76038	22	343	145	0.42	0.2780	8.0	0.38	8.9	0.00984	3.9	0.4		3330	125	63	2	44.8	2.5
34	0925RL-03_4	9856	76081	13	287	186	0.64	0.2030	10.4	0.244	11.2	0.00847	4.1	0.4		2830	170	54	2	43.7	2.3
35	0925RL-03_5	10070	76144	6	153	72	0.46	0.1870	8.7	0.225	9.4	0.00852	3.5	0.4		2670	143	55	2	45.1	1.9
36	0925RL-03_6	10103	76066	23	206	95	0.46	0.3660	10.2	0.62	12.7	0.01188	7.6	0.6		3700	155	76	6	45.6	5.0
37	0925RL-03_7	10210	75981	20	774	870	1.08	0.0667	5.4	0.0667	5.6	0.007264	1.5	0.3		800	113	47	1	45.5	0.7
38	0925RL-03_8	10260	75992	10	300	204	0.69	0.1470	11.0	0.171	11.4	0.00839	3.3	0.3	e	2270	188	54	2	47.1	1.9
39	0925RL-03_9	10370	75996	4	678	160	0.24	0.0543	3.2	0.053	3.4	0.0071	1.2	0.4		367	72	46	1	45.2	0.6
40	0925RL-03_10	10400	75969	17	725	161	0.22	0.1380	10.2	0.156	10.4	0.0082	2.1	0.2		2150	178	53	1	46.6	1.3
41	0925RL-03_11	10449	75992	9	522	407	0.80	0.0655	5.8	0.0679	6.0	0.007431	1.5	0.2		780	122	48	1	46.6	0.7
42	0925RL-03_12	10422	76035	8	307	172	0.56	0.1200	8.4	0.134	8.6	0.00798	1.8	0.2		1880	151	51	1	46.5	1.1
43	0925RL-03_13	10408	76121	16	371	253	0.69	0.2000	10.1	0.23	10.6	0.00835	3.4	0.3		2780	165	54	2	43.3	2.0
44	0925RL-03_14	10383	76168	13	261	226	0.87	0.2080	8.3	0.309	9.5	0.01076	4.8	0.5	r	2840	134	69	3	55.1	3.0
45	0925RL-03_15	10575	76068	22	349	283	0.80	0.2410	11.7	0.346	13.1	0.01004	6.0	0.5	e	3030	186	64	4	48.7	3.7
46	0925RL-03_16	10874	75964	12	139	56	0.43	0.3220	4.8	0.481	5.8	0.01072	3.1	0.5		3581	74	69	2	45.0	1.9
47	0925RL-03_17	10923	75870	9	147	72	0.49	0.2510	6.1	0.32	6.7	0.00937	2.7	0.4		3190	97	60	2	44.7	1.7
48	0925RL-03_18	11123	75894	11	286	136	0.45	0.1840	10.4	0.225	10.9	0.00868	3.4	0.3		2640	172	56	2	46.1	2.1
49	0925RL-03_19	11349	75915	7	403	177	0.44	0.0938	8.3	0.0973	8.5	0.00754	1.8	0.2		1460	157	48	1	45.6	0.9
50	0925RL-03_20	11091	75990	11	191	87	0.45	0.2520	11.6	0.344	12.4	0.00991	4.5	0.4	e	3150	183	64	3	47.2	3.1
51	0925RL-03_21	10593	76112	15	431	408	0.96	0.1360	10.4	0.164	10.8	0.00847	2.9	0.3	e	2160	181	54	2	48.3	1.7
52	0925RL-03_22	9664	76203	41	870	1330	1.47	0.1550	6.6	0.204	7.4	0.00942	3.3	0.5	r	2350	112	61	2	52.2	1.9
53	0925RL-03_23	10092	76103	7	148	66	0.44	0.2330	8.7	0.303	9.6	0.00929	4.2	0.4		3060	139	60	3	45.7	2.4
54	0925RL-03_24	10237	75984	2	219	90	0.39	0.0542	7.1	0.0535	8.1	0.00715	3.8	0.5		350	160	46	2	45.5	1.7
55	0925RL-03_25	10433	76013	6	333	198	0.60	0.0761	7.9	0.0787	8.0	0.00747	1.6	0.2		1030	157	48	1	46.2	0.8
56	0925RL-03_26	10583	76088	94	437	312	0.70	0.5120	3.7	1.19	7.2	0.0166	6.1	0.9		4273	55	106	6	44.3	3.7
57	0925RL-03_27	10396	76144	38	326	316	0.97	0.3760	8.1	0.67	11.0	0.01278	7.5	0.7	e	3820	122	82	6	48.1	4.8
58	0925RL-03_28	10908	75900	20	140	56	0.38	0.4460	4.5	0.879	6.8	0.01421	5.1	0.8		4088	66	91	5	45.4	3.2
59	0925RL-03_29	11113	75921	16	213	93	0.40	0.2840	5.8	0.389	6.5	0.01005	3.0	0.5		3386	90	65	2	45.3	1.9
60	0925RL-03_30	11101	75962	28	172	54	0.31	0.4200	8.9	0.86	11.7	0.0145	7.7	0.7	e	3950	133	93	7	49.4	5.7
216	0925RL-03Large_1	47863	77094	1	80	26	0.34	0.0580	8.4	0.0589	8.6	0.00726	1.8	0.2		470	184	47	1	46.0	0.9
217	0925RL-03Large_2	47657	77118	9	198	100	0.52	0.2100	9.6	0.263	10.5	0.00873	4.1	0.4		2850	156	56	2	44.5	2.3
218	0925RL-03Large_3	47378	77180	1	114	35	0.31	0.0496	6.6	0.0476	6.8	0.00697	1.7	0.3		190	153	45	1	44.6	0.8
219	0925RL-03Large_4	46986	77296	1	136	39	0.30	0.0507	6.1	0.0521	6.4	0.00735	2.2	0.3	e	270	140	47	1	47.0	1.0
220	0925RL-03Large_5	46153	77189	4	151	71	0.48	0.1570	7.8	0.172	8.6	0.00806	3.6	0.4		2410	132	52	2	44.6	1.8
221	0925RL-03Large_6	44853	77220	3	270	112	0.40	0.0493	4.6	0.0475	5.4	0.00697	2.8	0.5		159	109	45	1	44.6	1.2
222	0925RL-03Large_7	44905	77058	1	145	38	0.25	0.0486	6.1	0.0501	6.8	0.00732	2.9	0.4	e	160	144	47	1	46.9	1.4
223	0925RL-03Large_8	44381	77205	9	261	130	0.47	0.1610	9.4	0.19	10.2	0.00829	3.9	0.4		2400	159	53	2	45.6	2.0
224	0925RL-03LaCte_9	44042	77233	7	389	291	0.73	0.0570	4.4	0.0561	5.0	0.00718	2.3	0.5		462	97	46	1	45.5	1.1
225	0925RLB3Large_10	43523	77256	7	264	141	0.56	0.1230	5.2	0.1387	5.9	0.00826	2.7	0.5	e	2024	92	53	1	48.0	1.4
226	0925RL-03Large_11	43696	76995	3	310	160	0.50	0.0490	3.5	0.0486	4.1	0.00718	2.2	0.5		144	82	46	1	46.0	1.0
227	0925RL-03Large_12	43803	76945	5	198	91	0.46	0.1318	6.6	0.145	7.0	0.00796	2.2	0.3		2120	115	51	1	45.7	1.2
228	0925RL-03Large_13	43185	77199	2	300	69	0.24	0.0537	4.8	0.0521	5.3	0.00725	2.1	0.4		357	109	47	1	46.2	1.0
229	0925RL-03Large_14	43019	77058	3	193	95	0.50	0.0870	8.2	0.0879	8.7	0.00745	3.0	0.3		1300	157	48	1	45.4	1.4
230	0925RL-03Large_15	42735	77045	2	173	71	0.43	0.0471	5.7	0.0454	6.4	0.00703	2.9	0.5		70	135	45	1	45.1	1.3
231	0925RL-03Large_16	42773	77203	4	214	186	0.88	0.0758	10.0	0.0818	10.2	0.00779	2.2	0.2	r	950	200	50	1	48.2	1.1
232	0925RL-03Large_17	42577	77136	3	273	143	0.54	0.0522	4.0	0.0508	4.4	0.007108	1.7	0.4		276	92	46	1	45.4	0.8
233	0925RL-03Large_18	41806	76986	6	311	222	0.73	0.0835	5.4	0.0838	5.7	0.007322	1.6	0.3		1240	106	47	1	44.9	0.8
234	0925RL-03Large_19	41521	77216	4	176	91	0.50	0.1211	7.0	0.13	7.4	0.00794	2.5	0.3		1930	124	51	1	46.2	1.3
235	0925RL-03Large_20	41276	76994	4	331	186	0.58	0.0625	6.1	0.0614	6.3	0.00715	1.7	0.3		640	129	46	1	45.0	0.8
236	0925RL-03Large_21	41173	77018	5	156	96	0.63	0.1550	14.3	0.188	14.6	0.00859	3.3	0.2	e	2210	242	55	2	47.6	2.2
237	0925RL-03Large_22	41013	77181	14	318	152	0.49	0.2110	11.4	0.268	12.2	0.00915	4.2	0.3		2810	185	59	2	46.6	2.6
238	0925RL-03Large_23	40600	77388	4	332	198	0.61	0.0539	3.9	0.0534	4.2	0.007209	1.4	0.3		361	89	46	1	45.9	0.7
239	0925RL-03Large_24	40357	77048	2	177	81	0.44	0.0523	4.4	0.0512	4.8	0.00722	1.8	0.4		295	100	46	1	46.1	0.8
240	0925RL-03Large_25	40198	77038	4	208	98	0.48	0.0881	9.8	0.093	10.1	0.00744	2.3	0.2		1280	189	48	1	45.3	1.1
241	0925RL-03Large_26	39863	77091	2	234	123	0.54	0.0486	4.5	0.047	4.8	0.007062	1.7	0.3		128	106	45	1	45.3	0.8
242	0925RL-03Large_27	39621	77053	3	183	84	0.43	0.1012	6.8	0.1038	7.2	0.00752	2.2	0.3		1660	127	48	1	45.0	1.1
243	0925RL-03Large_28	39408	77038	1	148	43	0.29	0.0681	6.3	0.0662	6.5	0.007138	1.7	0.3		870	131	46	1	44.6	0.8
244	0925RL-03Large_29	39164	77140	4	230	105	0.46	0.0932	8.2	0.0948	8.3	0.00744	1.7	0.2		1440	154	48	1	45.0	0.9
245	0925RL-03Large_30	39388	77325	1	141	37	0.25	0.0491	5.7	0.0453	6.0	0.00692	2.0	0.3		160	132	44	1	44.3	0.9

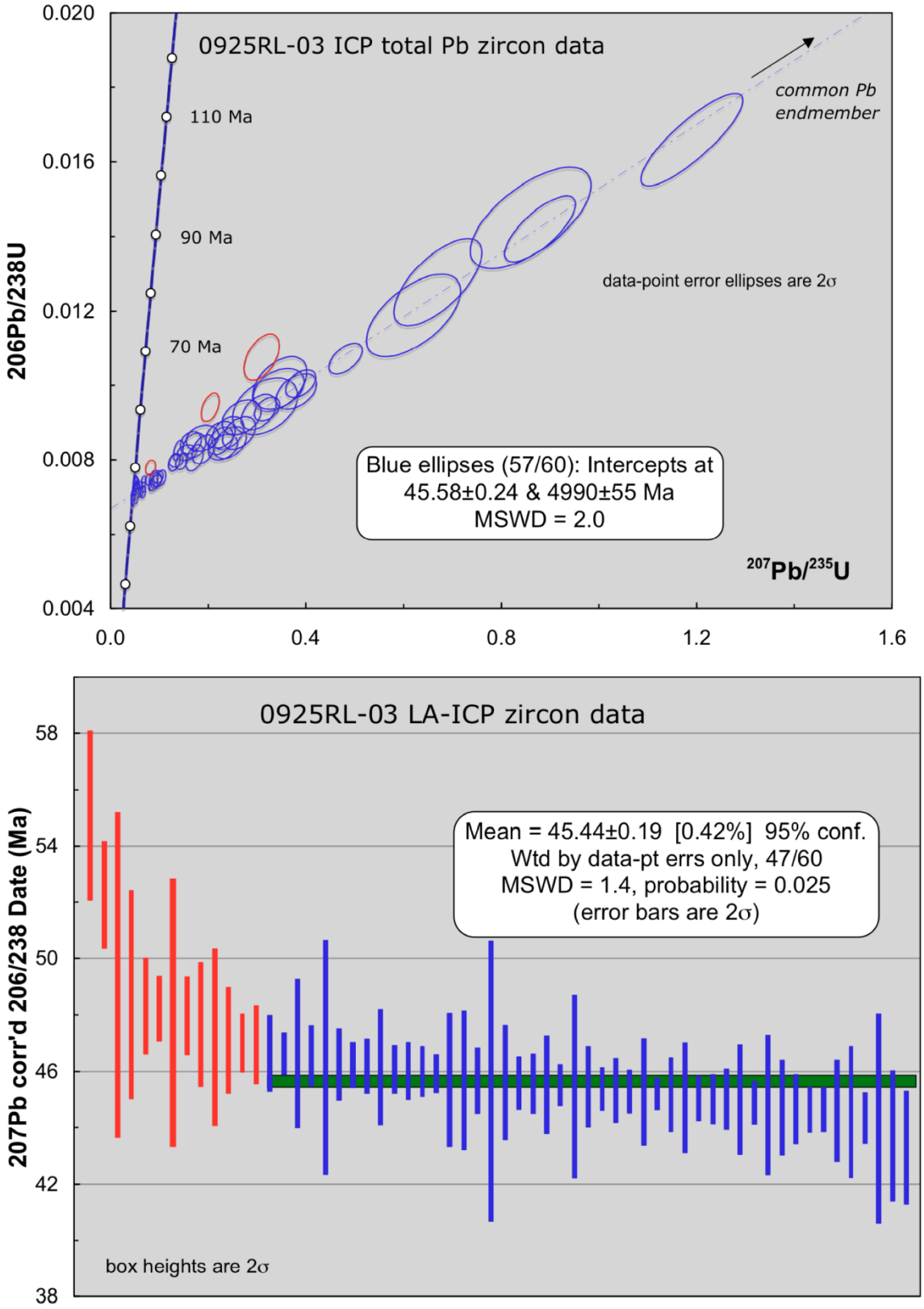

Figure A2-3. Data plots for 20150925RL-03, white lapilli tuff. Weighted mean ^{207}Pb-corrected ^{206}Pb/^{238}U date of 45.44±0.19 Ma is interpreted as best age of volcanism in this sample.

Table A2-2. Sample 150925RL-04, 45.23±0.23 Ma 95 percent confidence, weighted mean ^{207}Pb-corr. ^{206}Pb/^{238}U date (MSWD 1.2), 23/50 spots. Data acquired by laser ablation ICP-MS at UC Santa Barbara, March 2016. All ratios and dates are total Pb, which includes common Pb, except the column labelled 207Pb-corrected. excl. = data excluded from calculated date: r = red ellipses on concordia plots, e = additional excluded from weighted mean calculation, *A = Archean detrital grains.

order	sample name spot#	X	Y	Pb (ppm)	U (ppm)	Th (ppm)	Th/U	207/206	2SE %	207/235	2SE %	206/238	2SE %	Rho	excl.	207/206 Date (Ma)	2 SE abs.	206/238 Date (Ma)	2 SE abs.	207Pb corr'd 206/238 Date (Ma)	2 SE abs.
61	0925RL-04_1	14692	78001	16	412	214	0.52	0.1770	6.9	0.22	7.6	0.00895	3.2	0.4	e	2600	115	57	2	48.0	1.8
62	0925RL-04_2	14687	78041	8	578	372	0.53	0.0570	4.2	0.0587	4.7	0.00754	2.1	0.4	e	463	93	48	1	47.8	1.0
63	0925RL-04_3	14818	78057	23	500	258	0.51	0.2040	7.0	0.25	7.4	0.00887	2.6	0.3		2820	114	57	1	45.7	1.6
64	0925RL-04_4	14831	78033	24	514	269	0.51	0.1910	10.6	0.243	11.3	0.00876	4.0	0.4		2720	173	56	2	46.0	2.3
65	0925RL-04_5	15028	78034	17	553	149	0.25	0.1661	5.2	0.193	5.5	0.00839	1.9	0.4		2505	87	54	1	45.8	1.1
66	0925RL-04_6	15041	78108	6	370	72	0.19	0.0981	8.2	0.104	8.4	0.0077	1.9	0.2	e	1500	152	49	1	46.3	1.0
67	0925RL-04_7	14755	77891	12	527	137	0.26	0.1250	7.6	0.136	7.8	0.00797	2.0	0.3		2020	134	51	1	46.1	1.1
68	0925RL-04_8	14753	77832	4	466	126	0.27	0.0617	4.1	0.0616	4.3	0.007204	1.3	0.3		637	88	46	1	45.4	0.6
69	0925RL-04_9	14908	77795	23	497	374	0.74	0.1860	7.6	0.244	8.1	0.00928	2.7	0.3	e	2700	126	60	2	49.1	1.7
70	0925RL-04_10	15040	77810	13	552	176	0.31	0.1310	10.0	0.151	10.2	0.00814	2.0	0.2	e	2040	176	52	1	46.7	1.3
71	0925RL-04_11	15041	77898	15	477	171	0.35	0.1649	4.2	0.186	4.7	0.00848	2.2	0.5	e	2515	70	54	1	46.4	1.1
72	0925RL-04_12	15139	77815	8	539	215	0.39	0.0833	10.6	0.093	10.9	0.00788	2.2	0.2	e	1110	208	51	1	48.3	1.2
73	0925RL-04_13	15280	77804	12	713	408	0.48	0.0827	10.2	0.086	10.5	0.00733	2.3	0.2		1200	200	47	1	45.0	1.1
74	0925RL-04_14	15507	77782	12	934	270	0.28	0.0829	6.4	0.0819	6.7	0.00734	1.8	0.3		1260	125	47	1	45.0	0.9
75	0925RL-04_15	15755	77771	9	529	370	0.38	0.0900	13.4	0.099	13.9	0.00784	3.7	0.3	e	1260	256	50	2	47.6	1.9
76	0925RL-04_16	15755	77829	9	483	135	0.27	0.1030	11.7	0.115	11.9	0.00794	2.1	0.2	e	1560	217	51	1	47.4	1.3
77	0925RL-04_17	15958	77871	14	886	266	0.30	0.0979	6.4	0.1001	6.6	0.007435	1.7	0.3		1600	119	48	1	44.7	0.8
78	0925RL-04_18	16125	77900	77	339	199	0.55	0.5240	6.2	1.35	11.3	0.0181	9.4	0.8	e	4300	92	115	11	46.6	6.4
79	0925RL-04_19	16371	77895	20	344	209	0.59	0.2330	8.7	0.291	9.3	0.00904	3.4	0.4		3050	139	58	2	44.4	2.1
80	0925RL-04_20	16412	77824	18	431	164	0.38	0.1860	5.5	0.233	5.9	0.00908	1.9	0.3	e	2699	91	58	1	48.1	1.2
81	0925RL-04_21	16547	77858	5	497	180	0.37	0.0633	5.5	0.0645	5.8	0.007524	1.6	0.3	e	680	117	48	1	47.3	0.8
82	0925RL-04_22	16519	77929	12	367	126	0.34	0.1620	9.4	0.194	9.7	0.00855	2.7	0.3	e	2400	158	55	1	46.9	1.6
83	0925RL-04_23	16521	78146	12	758	309	0.40	0.0828	9.0	0.0799	9.2	0.00722	1.7	0.2		1260	176	46	1	44.3	0.9
84	0925RL-04_24	16663	78235	33	722	762	1.03	0.1720	10.5	0.19	11.0	0.00806	3.0	0.3		2590	176	52	2	43.6	1.8
85	0925RL-04_25	16520	78219	13	409	179	0.43	0.1500	12.1	0.17	12.6	0.00832	3.6	0.3	e	2230	206	53	2	46.5	2.1
86	0925RL-04_26	16203	78175	34	443	215	0.47	0.3000	12.7	0.452	14.6	0.01092	7.2	0.5	e	3350	197	70	5	47.8	4.8
87	0925RL-04_27	15747	78141	13	1162	764	0.63	0.0508	2.5	0.0497	2.9	0.007249	1.5	0.5	e	225	58	47	1	46.3	0.7
88	0925RL-04_28	15654	78059	9	255	193	0.73	0.1440	7.7	0.167	8.1	0.00841	2.3	0.3	e	2250	133	54	1	47.4	1.3
89	0925RL-04_29	15469	78085	6	498	169	0.33	0.0726	6.5	0.0722	6.7	0.00718	1.8	0.3		940	131	46	1	44.6	0.9
90	0925RL-04_30	15955	78139	15	881	254	0.29	0.1090	10.2	0.116	10.6	0.00771	2.9	0.3		1640	186	50	1	45.6	1.5
196	0925RL-04Large_1	45983	78530	10	1100	455	0.35	0.0476	2.2	0.0466	2.8	0.00712	1.7	0.6		77	52	46	1	45.7	0.8
197	0925RL-04Large_2	45726	78571	58	129	49	0.38	0.1798	1.4	12.06	2.1	0.4899	1.6	0.8	*A	2651	22	2570	42	2543.5	46.3
198	0925RL-04Large_3	45501	78591	4	412	133	0.33	0.0602	3.4	0.0643	3.9	0.00775	2.0	0.5	r	606	74	50	1	48.9	1.0
199	0925RL-04Large_4	45754	78816	5	512	127	0.25	0.0690	4.1	0.07	4.5	0.00732	1.7	0.4		914	85	47	1	45.7	0.8
200	0925RL-04Large_5	45244	78668	16	1085	727	0.68	0.0591	4.4	0.0574	4.8	0.00706	1.7	0.4		558	96	45	1	44.7	0.8
201	0925RL-04Large_6	44979	78722	5	581	190	0.31	0.0582	5.6	0.0608	6.0	0.00736	2.1	0.4	e	490	124	47	1	46.6	1.0
202	0925RL-04Large_7	44856	78648	24	789	516	0.66	0.1330	8.4	0.153	8.7	0.00815	2.5	0.3	e	2060	146	52	1	46.7	1.4
203	0925RL-04Large_8	44728	78659	25	516	177	0.34	0.2270	9.8	0.288	10.4	0.00907	3.7	0.4		3030	157	58	2	45.0	2.3
204	0925RL-04Large_9	44591	78460	110	78	95	1.23	0.1722	1.9	11.15	4.7	0.476	4.3	0.9	*A	2579	33	2507	108	2488.8	115.9
205	0925RL-04Large_10	44330	78576	133	95	108	1.14	0.1766	1.4	11.67	2.2	0.4756	1.7	0.8	*A	2621	23	2507	43	2473.2	46.5
206	0925RL-04Large_11	44201	78691	130	91	109	1.21	0.1772	1.4	11.71	2.4	0.4819	2.0	0.8	*A	2627	23	2535	50	2506.6	54.5
207	0925RL-04Large_12	44458	78804	2	344	90	0.26	0.0472	4.0	0.046	4.7	0.00705	2.4	0.5		72	96	45	1	45.3	1.1
208	0925RL-04Large_13	43558	78421	2	426	87	0.20	0.0479	3.4	0.048	3.9	0.0072	1.9	0.5	e	99	80	46	1	46.2	0.9
209	0925RL-04Large_14	43666	78588	2	415	89	0.21	0.0468	3.5	0.0457	4.3	0.00714	2.6	0.6		46	83	46	1	45.9	1.2
210	0925RL-04Large_15	43338	78618	19	865	370	0.42	0.1192	5.5	0.1276	5.9	0.0078	2.2	0.4		1938	99	50	1	45.5	1.1
211	0925RL-04Large_16	43243	78705	3	454	123	0.24	0.0488	3.9	0.049	4.6	0.00722	2.4	0.5	e	136	92	46	1	46.3	1.1
212	0925RL-04Large_17	43191	78436	7	667	204	0.31	0.0712	4.0	0.0717	4.3	0.007333	1.6	0.4		961	82	47	1	45.7	0.7
213	0925RL-04Large_18	43333	78541	7	417	148	0.37	0.1030	11.7	0.11	12.0	0.00761	2.3	0.2		1540	217	49	1	45.4	1.3
214	0925RL-04Large_19	43614	78479	2	333	94	0.29	0.0506	3.4	0.0494	3.9	0.00703	2.0	0.5		217	79	45	1	45.0	0.9
215	0925RL-04Large_20	45970	78840	1	141	24	0.18	0.0581	7.3	0.0601	7.7	0.00738	2.4	0.3	e	500	161	47	1	46.7	1.1

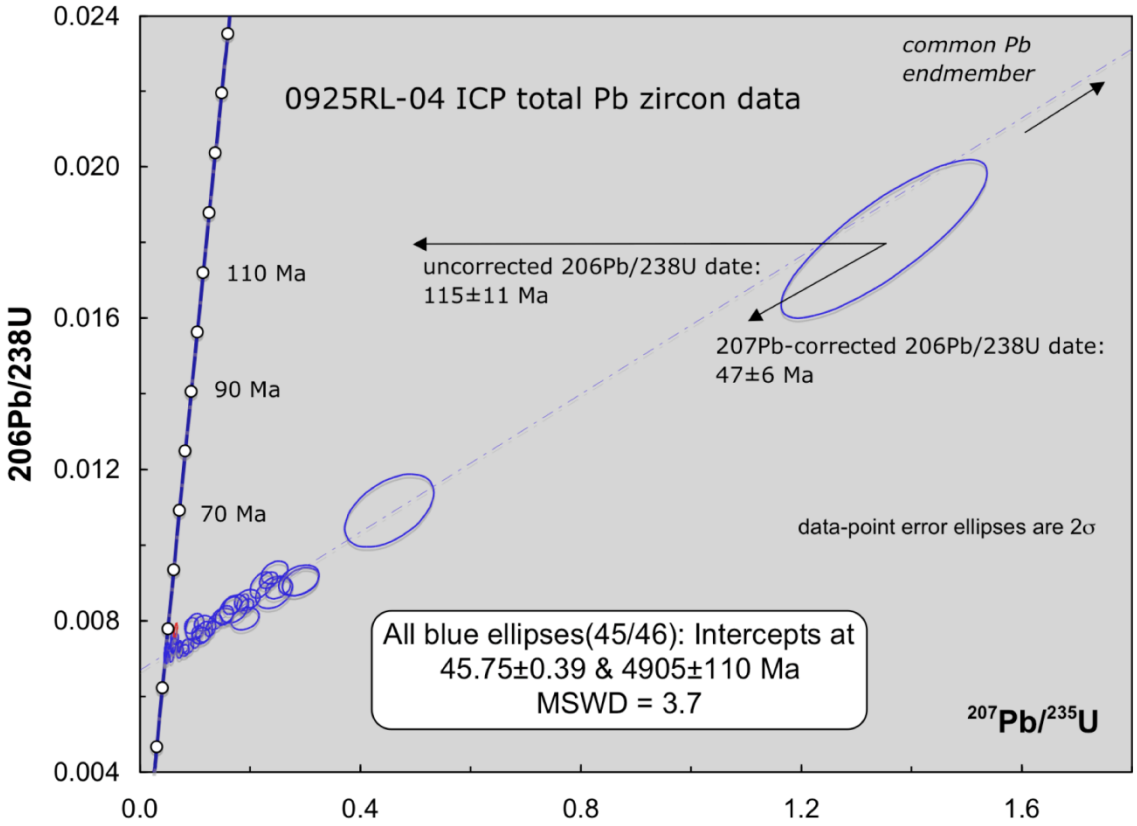

Figure A2-4. Concordia plot of total Pb data from 46 LA-ICP spots from 20150925RL-04, the upper crystalline flow, demonstrating the two methods for correction of common Pb. Discordance for Phanerozoic data on total Pb plots is generally interpreted to reflect varying proportions of common Pb. Magmatic ages can be determined by linear regression of data from coeval zircons by assuming there has been no Pb loss and that the zircons share a common Pb isotopic endmember. This method is demonstrated by the regression of 45 blue data points, with a lower intercept of 45.75±0.39 Ma interpreted as the magmatic age. The upper intercept has no age significance, but represents the common Pb endmember with a $^{207}Pb/^{206}Pb$ of 0.795±0.064. The ^{207}Pb-correction method is a variation on this model that can be applied to individual data points by assuming a common Pb $^{207}Pb/^{206}Pb$ and calculating the associated $^{206}Pb/^{238}U$ dates. For the annotated point, the ^{207}Pb-corrected date is 47±6 Ma, within error of the lower intercept of all 45 points. The uncorrected $^{206}Pb/^{238}U$ date for this point is considerably older, 115±11 Ma, indicating that there is a significant amount of common Pb in this zircon. With an MSWD significantly greater than 1, the linear regression has considerable scatter, so a weighted mean of select ^{207}Pb-corrected analyses is favored for the age of volcanism (fig. A2-5).

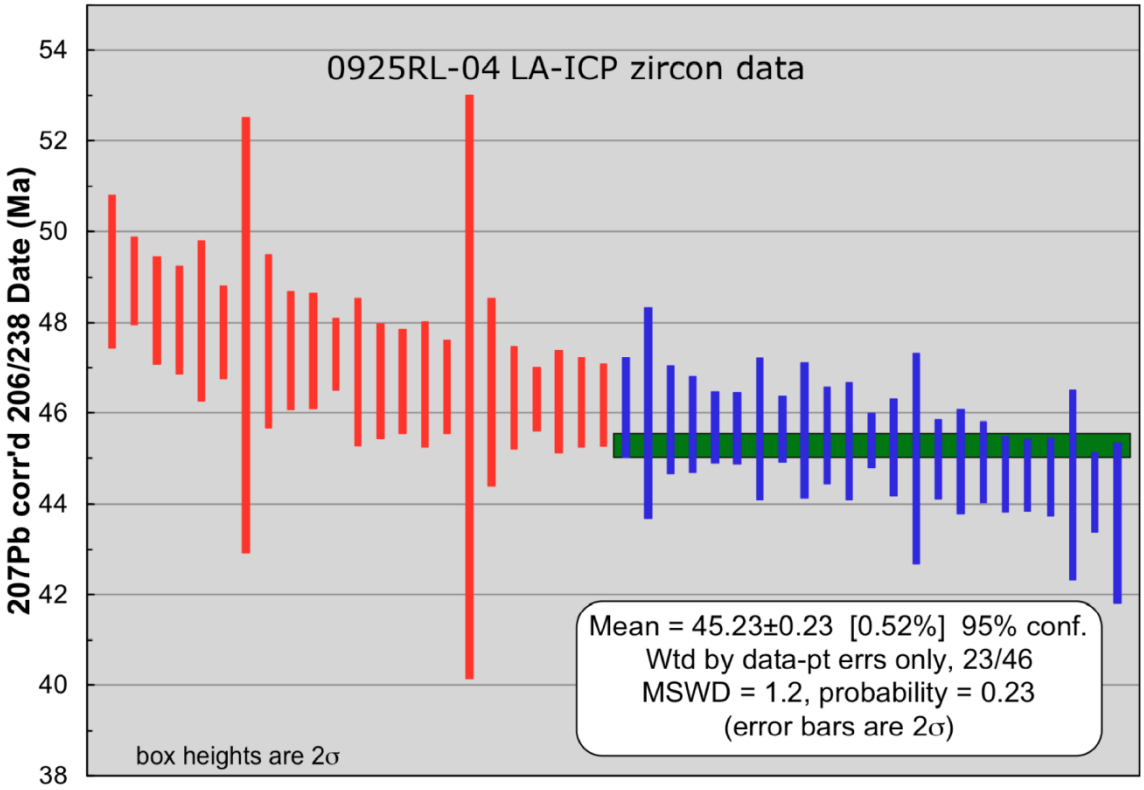

Figure A2-5. Weighted mean of ^{207}Pb-corrected ^{206}Pb/^{238}U dates from 20150925RL-04. A subset of the youngest 23 dates yields the highest precision and reasonable MSWD and is interpreted as the favored age for volcanism.

Table A2-3. Sample 150925RL-05, 47.88±0.28 Ma 95% confidence, weighted mean ^{207}Pb-corr. ^{206}Pb/^{238}U date (MSWD 1.0), 17/30 points. Data acquired by laser ablation ICP-MS at UC Santa Barbara, March 2016. All ratios and dates are total Pb, which includes common Pb, except the column labelled 207Pb-corrected. excl. = data excluded from calculated date: r = red ellipses on concordia plots, e = additional excluded from weighted mean calculation, *A = Archean detrital grains.

order	sample name spot#	X	Y	Pb (ppm)	U (ppm)	Th (ppm)	Th/U	207/206	2SE %	207/235	2SE %	206/238	2SE %	Rho	excl.	207/206 Date (Ma)	2 SE abs.	206/238 Date (Ma)	2 SE abs.	207Pb corr'd 206/238 Date (Ma)	2 SE abs.
91	0925RL-05_1	12819	77872	6	165	151	0.89	0.1540	13.7	0.185	14.1	0.00867	3.4	0.2		2280	233	56	2	48.2	2.2
92	0925RL-05_2	12496	78065	19	177	162	0.88	0.3200	7.3	0.507	8.3	0.0115	3.9	0.5		3610	112	74	3	48.4	2.9
93	0925RL-05_3	12465	77932	20	167	129	0.74	0.3680	6.7	0.636	8.7	0.01241	5.6	0.6		3780	101	80	4	47.5	3.6
94	0925RL-05_4	12276	78161	10	131	111	0.83	0.2510	7.7	0.369	8.2	0.01055	2.9	0.4	r	3180	122	68	2	50.3	2.2
95	0925RL-05_5	12138	78058	11	239	289	1.19	0.1620	6.9	0.201	7.3	0.00906	2.3	0.3	r	2490	117	58	1	49.7	1.4
96	0925RL-05_6	11926	78073	12	274	417	1.49	0.1248	8.0	0.135	8.4	0.00794	2.4	0.3		2000	142	51	1	46.0	1.3
97	0925RL-05_7	12053	78116	9	280	324	1.14	0.1024	7.8	0.117	8.0	0.00824	1.8	0.2	r	1630	145	53	1	49.2	1.0
98	0925RL-05_8	11611	78235	6	117	92	0.77	0.2000	13.1	0.248	13.5	0.00915	3.3	0.2		2800	213	59	2	47.4	2.5
99	0925RL-05_9	11726	78103	6	163	150	0.88	0.1500	11.4	0.2	12.1	0.0094	4.1	0.3	r	2260	195	60	2	52.5	2.5
100	0925RL-05_10	11513	78077	11	445	354	0.77	0.0783	10.7	0.09	11.1	0.00824	2.9	0.3	r	1010	212	53	2	50.8	1.5
101	0925RL-05_11	11406	78296	34	145	121	0.85	0.5110	8.5	1.52	14.1	0.0188	11.2	0.8	r	4250	125	120	13	50.4	8.6
102	0925RL-05_12	11205	78129	5	179	160	0.88	0.0920	10.9	0.108	11.2	0.00826	2.5	0.2	r	1300	208	53	1	50.0	1.4
103	0925RL-05_13	11059	78286	6	140	155	1.08	0.1580	10.2	0.204	10.8	0.00921	3.4	0.3	r	2370	173	59	2	50.9	2.1
104	0925RL-05_14	10655	78135	11	178	137	0.77	0.2390	4.8	0.336	5.3	0.01017	2.4	0.4	r	3112	76	65	2	49.5	1.5
105	0925RL-05_15	10611	78303	5	307	126	0.35	0.0930	10.8	0.101	11.1	0.00787	2.4	0.2		1370	205	51	1	47.6	1.3
106	0925RL-05_16	10510	78290	17	131	119	0.90	0.4110	4.3	0.762	5.8	0.01343	3.9	0.7		3949	65	86	3	46.7	2.6
107	0925RL-05_17	10256	78193	6	395	285	0.73	0.0482	3.0	0.0494	3.3	0.007531	1.4	0.4		101	71	48	1	48.3	0.7
108	0925RL-05_18	9981	78276	6	251	249	0.98	0.0727	5.9	0.0769	6.1	0.00767	1.6	0.3		950	120	49	1	47.7	0.8
109	0925RL-05_19	9912	78426	4	196	181	0.92	0.0535	5.4	0.0559	5.5	0.007598	1.3	0.2		320	122	49	1	48.4	0.6
110	0925RL-05_20	9687	78358	14	384	465	1.17	0.1051	4.6	0.1163	4.8	0.00806	1.6	0.3		1737	84	52	1	48.0	0.8
111	0925RL-05_21	9564	78112	5	211	173	0.81	0.0782	6.7	0.0812	6.9	0.00767	2.0	0.3		1120	132	49	1	47.3	1.0
112	0925RL-05_22	9523	78398	24	85	49	0.56	0.5600	4.3	1.64	8.1	0.0205	6.9	0.8		4394	63	131	9	46.9	5.1
113	0925RL-05_23	9523	78280	8	216	172	0.80	0.1450	13.9	0.17	14.3	0.00829	3.5	0.2		2140	238	53	2	46.7	2.1
114	0925RL-05_24	9633	78403	10	291	185	0.63	0.1440	11.2	0.167	11.5	0.00846	2.8	0.2		2200	193	54	2	47.7	1.7
115	0925RL-05_25	12282	77997	52	105	73	0.69	0.6730	2.7	2.76	6.6	0.0301	6.1	0.9		4677	39	191	12	42.3	5.0
116	0925RL-05_26	11700	78216	4	149	145	0.97	0.0962	7.7	0.1093	8.0	0.00832	2.3	0.3	r	1510	145	53	1	50.1	1.2
117	0925RL-05_27	12109	78209	5	184	184	0.99	0.0931	8.9	0.103	9.2	0.00806	2.4	0.3	r	1490	169	52	1	48.7	1.3
118	0925RL-05_28	12156	78101	7	203	216	1.04	0.1220	10.7	0.142	11.0	0.00844	2.6	0.2	r	1920	191	54	1	49.1	1.5
119	0925RL-05_29	12278	78093	3	109	71	0.64	0.1250	9.7	0.146	10.0	0.00846	2.4	0.2	r	1940	172	54	1	49.0	1.4
120	0925RL-05_30	12480	77987	6	196	169	0.84	0.1200	10.9	0.139	11.2	0.00821	2.6	0.2		1870	195	53	1	47.9	1.5

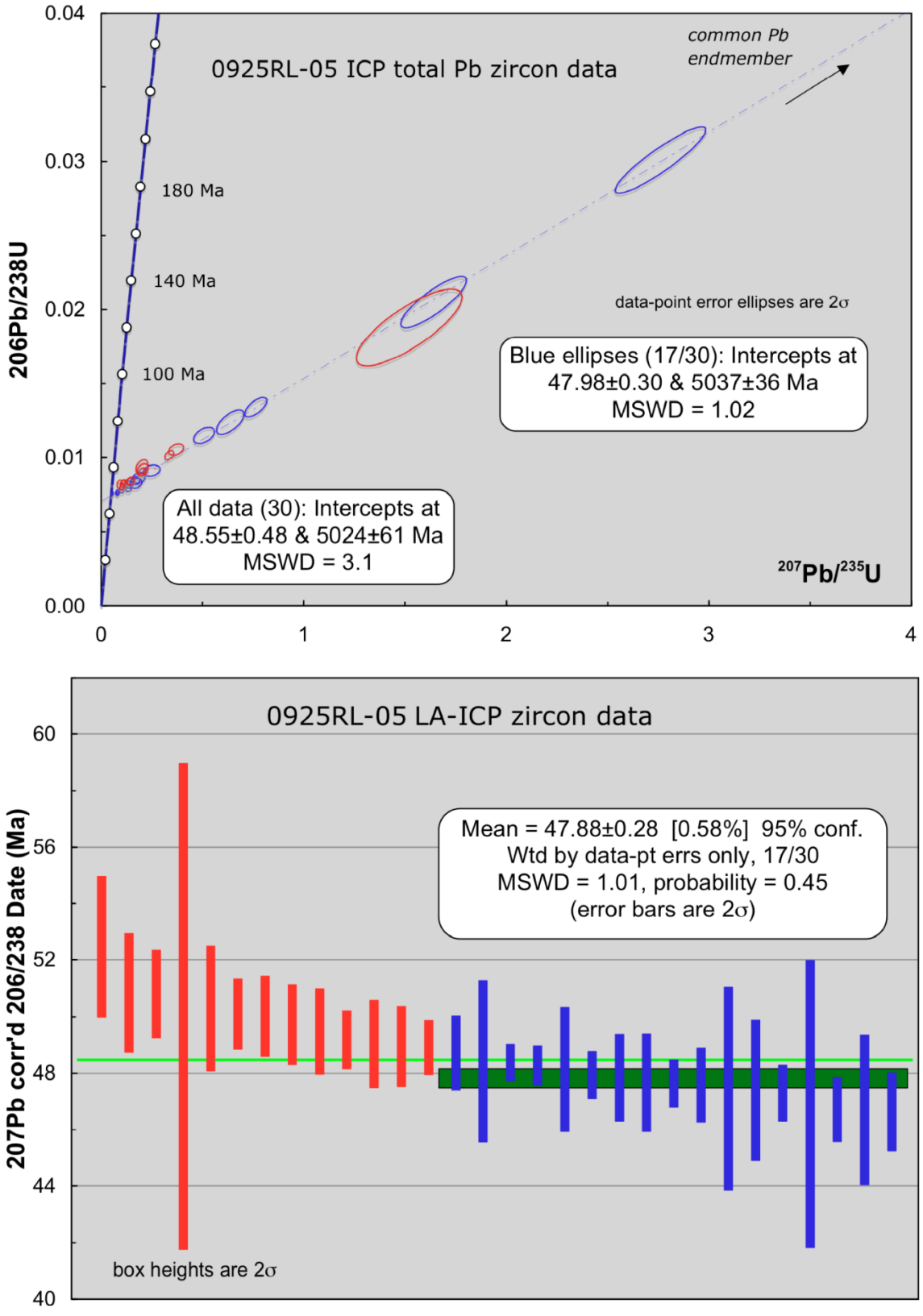

Figure A2-6. Data plots for 20150925RL-05, basal yellow tuff. Weighted mean ^{207}Pb-corrected ^{206}Pb/^{238}U date of 47.88±0.28 Ma is interpreted as best age of volcanism in this sample.

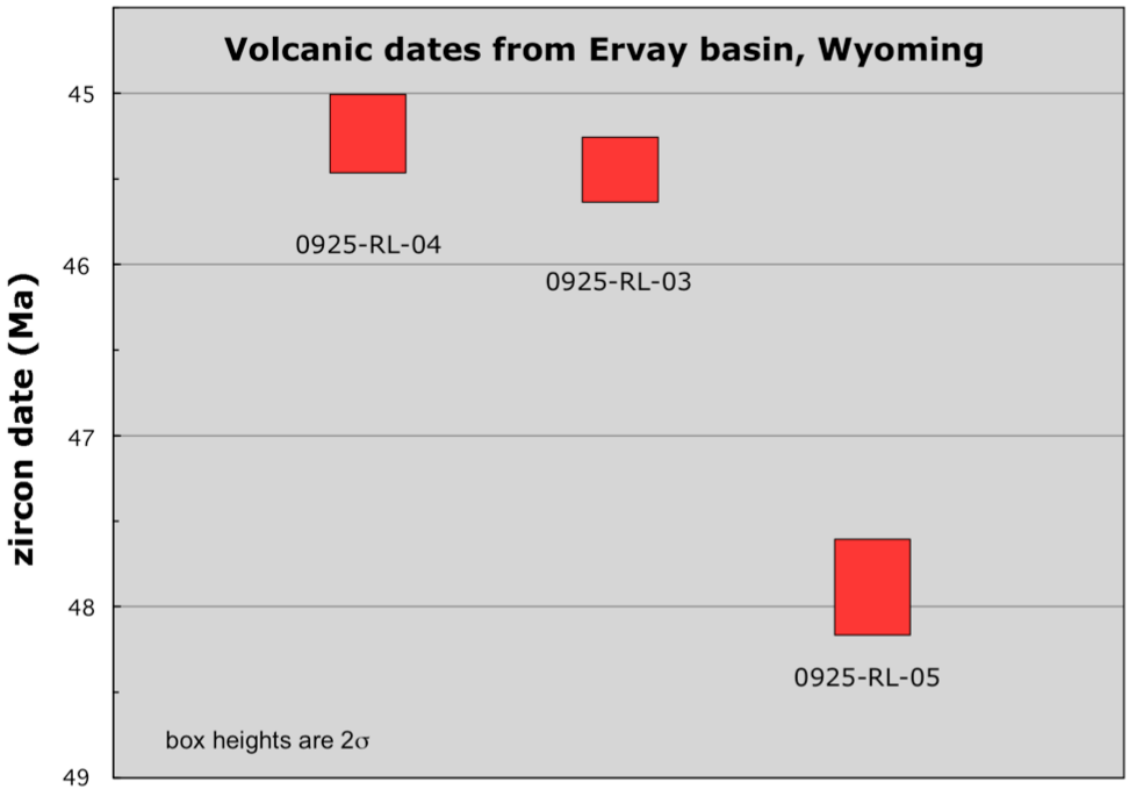

Figure A2-7. Summary plot of the three weighted mean ^{207}Pb-corrected ^{206}Pb/^{238}U LA-ICP dates on volcanism. Samples are ordered from highest in section on the left to lowest on the right. Dates on the upper two samples overlap within error although there could be a maximum of 0.63 Ma between them at the limits of uncertainty. Differences in volcanic ages between the lower two samples range from a minimum of 1.97 Ma to a maximum of 2.91 Ma.

APPENDIX 3: GEOCHRONOLOGIC EVALUATION OF SAMPLE 20150925RL-07

Report by:

Kevin R. Chamberlain, Research Professor, University of Wyoming, August 15, 2016

Executive Summary

CATIMS zircon and ID-TIMS dark titanite analyses of French Rocks tonalite establish a magmatic age of 2,655±3 Ma, similar to those of the associated Sage Hen Intrusive suite. This supports constraints on the earliest phase of deformation on the nearby Oregon Trail structural belt (OTSB) ca. 2.65 Ga. ID-TIMS analyses of pale titanite date the timing of deformation of the French Rocks tonalite to 2,630±2 Ma, again supporting previous constraints on the second phase of deformation in the OTSB.

Methods

The rock sample was crushed mechanically, and heavy minerals were concentrated by a Wilfley shaker table separation. Zircons and titanite grains were further purified by magnetic separation and heavy liquid flotation of lighter minerals.

Zircons were generally euhedral, metamict and bimodal in size (fig. A3-1) with large to extra-large grains (200-300 μm in length) and a distinct population of small, equant grains (30 to 50 μm). Representative populations of both sizes were selected for annealing and U-Pb dating.

Selected zircons were annealed at 850°C for 50 hours, then dissolved in two steps in a chemical abrasion, thermal ionization mass spectrometric U-Pb dating method (CA-TIMS) modified from Mattinson (2005). The first dissolution step was in hydrofluoric acid (HF) and nitric acid (HNO_3) at 180°C for 12 hours. This removed the most metamict zircon domains in the annealed crystals (fig. A3-2). Individual grains were then spiked with a mixed ^{205}Pb-^{233}U-^{235}U tracer (ET535), completely dissolved in HF and HNO_3 at 240°C for 30 hours, and then converted to chlorides. The dissolutions were loaded onto rhenium filaments with phosphoric acid and silica gel without any further chemical processing. Pb and UO_2 isotopic compositions were determined in single Daly-photomultiplier mode on a Micromass Sector 54 mass spectrometer. Data were reduced and ages calculated using PbMacDat and ISOPLOT/EX after Ludwig (1988, 1991). Total common Pb varied from 3.5 to 0.4 picograms and was all assigned to blank.

Two distinct colors of titanite (fig. A3-3) were also recovered and dated. Dark titanite generally forms at higher temperatures than pale titanite (Frost and others, 2000), so each growth may represent different processes. This sample is foliated and was collected from near the TSB (Grace and others, 2006), so the dark titanite could represent either magmatic growth or high temperature metamorphic growth during deformation. Pale grains are likely metamorphic growth at lower temperature. Grains of each color were processed separately to test for distinct dates.

Titanite grains were spiked with ET535 tracer and dissolved in an HCl:HF mix of 5:1 at 180°C for 30 hours. Pb and U were purified from solution on ion exchange resins using HCl-HBr methods adapted from Tilton (1973) with an HNO_3-HCl clean-up column to further purify U. Pb was loaded on rhenium filaments with silica gel. U was loaded on separate filaments with graphite and run as a metal. Isotopic compositions of Pb and U were determined in multi-collector, Faraday mode using the Daly multiplier for ^{204}Pb when the $^{206}Pb/^{204}Pb$ was greater

than 200. Procedural blanks averaged 4 picograms Pb and 0.1 picograms U. The data were corrected for common Pb in titanite in excess of blank using both model initial Pb isotopic compositions and a total Pb $^{206}Pb/^{204}Pb$ vs $^{207}Pb/^{204}Pb$ isochron approach.

Results

Four single, partially-dissolved zircons were spiked, completely dissolved, and analyzed for U-Pb data. These included one small grain (50x50 microns), one large grain (200x100 microns) and the tips of two large grains (100x100x20 microns each). The two tips were selected to make sure to avoid any potential older cores. Data from all four analyses overlapped each other and concordia (table A3-1, fig. A3-4). The Concordia Age (Ludwig 1998) combines both the $^{206}Pb/^{238}U$ and $^{207}Pb/^{235}U$ dates and includes the uncertainties in the uranium decay constants. For these data, the Concordia Age is 2,654±5 Ma. Weighted mean $^{207}Pb/^{206}Pb$ date from these four analyses is 2,655±3 Ma (table A3-1, fig. A3-5), which is interpreted as the best estimate for the intrusive age of this pluton.

Two picks each of dark and pale titanite were analyzed (fig. A3-3). The $^{206}Pb/^{204}Pb$ of the pale large pick (p3) was high enough (609, table A3-1) that the calculated concordia intercepts and $^{207}Pb/^{206}Pb$ date are relatively insensitive to the choice of initial Pb isotopic compositions, but for the other three analyses, this choice can affect the calculated ages by several tens of million years (Verts and others, 1996). Consequently, two approaches were compared to correct for the common Pb from titanite: 1) using model Pb isotopic compositions, and 2) a total Pb isochron approach that does not require estimations of initial Pb isotopic compositions. The model Pb isotopic compositions used to calculate concordia intercepts had slightly elevated $^{207}Pb/^{204}Pb$ values relative to the Stacey and Kramers (1975) model (14.90 vs. 14.739 at 2,650 Ma, with 13.74 for $^{206}Pb/^{204}Pb$), consistent with those of measured whole rock Pb isotopic compositions for the Wyoming province (e.g. Frost and others, 2006a, b). The calculated $^{207}Pb/^{206}Pb$ dates from the two dark analyses converge ca. 2,657 Ma despite variation in $^{206}Pb/^{204}Pb$ (168 and 58, table 1) suggesting that this choice of initial Pb isotopic compositions is appropriate for the initial Pb component of the dark titanite. The total Pb, $^{207}Pb/^{204}Pb$ vs. $^{206}Pb/^{204}Pb$ isochron approach yields a date of 2,654±8 Ma (table A3-2, fig. A3-6) and initial $^{207}Pb/^{204}Pb$ of 14.94 at $^{206}Pb/^{204}Pb$ of 13.74. Although linearity cannot be tested with only two analyses, the agreement in dates between the two common Pb correction methods supports an age of ca. 2,654 Ma for the crystallization age of dark titanite. As the Pb/Pb isochron method is independent of choosing an initial Pb isotopic composition, its date of 2,654±8 Ma is interpreted as the best estimate of the crystallization age of dark titanite. This age is within error of the zircon date (fig. A3-5), so the dark titanite grains are interpreted as magmatic growth.

The two pale titanite analyses yielded consistent $^{207}Pb/^{206}Pb$ dates of ca. 2630 Ma (table A3-1) when corrected for initial Pb of 13.797, 15.01, 33.513 for $^{206}Pb/^{204}Pb$, $^{207}Pb/^{204}Pb$ and $^{208}Pb/^{204}Pb$, respectively. These values have slightly elevated $^{207}Pb/^{204}Pb$ compared to Stacey and Kramers (1975) model for 2,630 Ma. The isotope dilution data from pick 4 was uninterpretable as the sample to tracer ratio was too high, so only Pb isotopic data are available for that sample. The data from large pale p3 are concordant and relatively insensitive to the choice of initial Pb isotopic composition due to the high $^{206}Pb/^{204}Pb$ value. The total Pb, $^{207}Pb/^{204}Pb$ vs. $^{206}Pb/^{204}Pb$ isochron approach yields a date of 2,629±13 Ma (table A3-2, fig. A3-6) and initial $^{207}Pb/^{204}Pb$ of 15.01 at $^{206}Pb/^{204}Pb$ of 13.80. The best estimate for the crystallization age of the pale titanite is 2,630.3±1.9 Ma based on the weighted mean $^{207}Pb/^{206}Pb$ date of the two points.

Discussion

The magmatic age of 2,655±3 Ma for the French Rocks tonalite is similar to those of several other nearby intrusions, such as the Circle Bar Ranch granite, Middle Sage Hen quartz diorite, and East Sage Hen granite (Langstaff ,1995; Fruchey, 2002), an association that Langstaff (1995) named the Sage Hen Intrusive suite. As a whole, these foliated plutons post-date the earliest deformational fabrics in the Barlow Gap region to the south of the Ervay basin quad, but contain the second fabric (Fruchey, 2002).

Deformation in the Barlow gap region is part of the Oregon Trail structural belt (Chamberlain and others, 2003; Grace and others, 2006), a ~20 km wide, east-west trending high-strain zone that represents the collisional suture between the ancient core of the Wyoming craton in the north, to the Southern Accreted terranes and Superior province in the south (Grace and others, 2006; Chamberlain and others, 2015; Kilian and others, 2015; Parker and others, 2015). Two phases of deformation in the Oregon Trail structural belt have been directly dated by the ages of syn-deformational titanite and metamorphic zircon at ca. 2.65 and 2.63 Ga (Fruchey, 2002; Grace and others, 2006; Frost and others, 2006c; Chamberlain, unpub. data).

The pale titanite date in the French Rocks tonalite matches the age of the second deformation in the Oregon Trail structural belt. This establishes that deformation associated with the suture propagated north of the high-strain zone and affected much of the ancient core of the Wyoming craton (Parker and others, 2015).

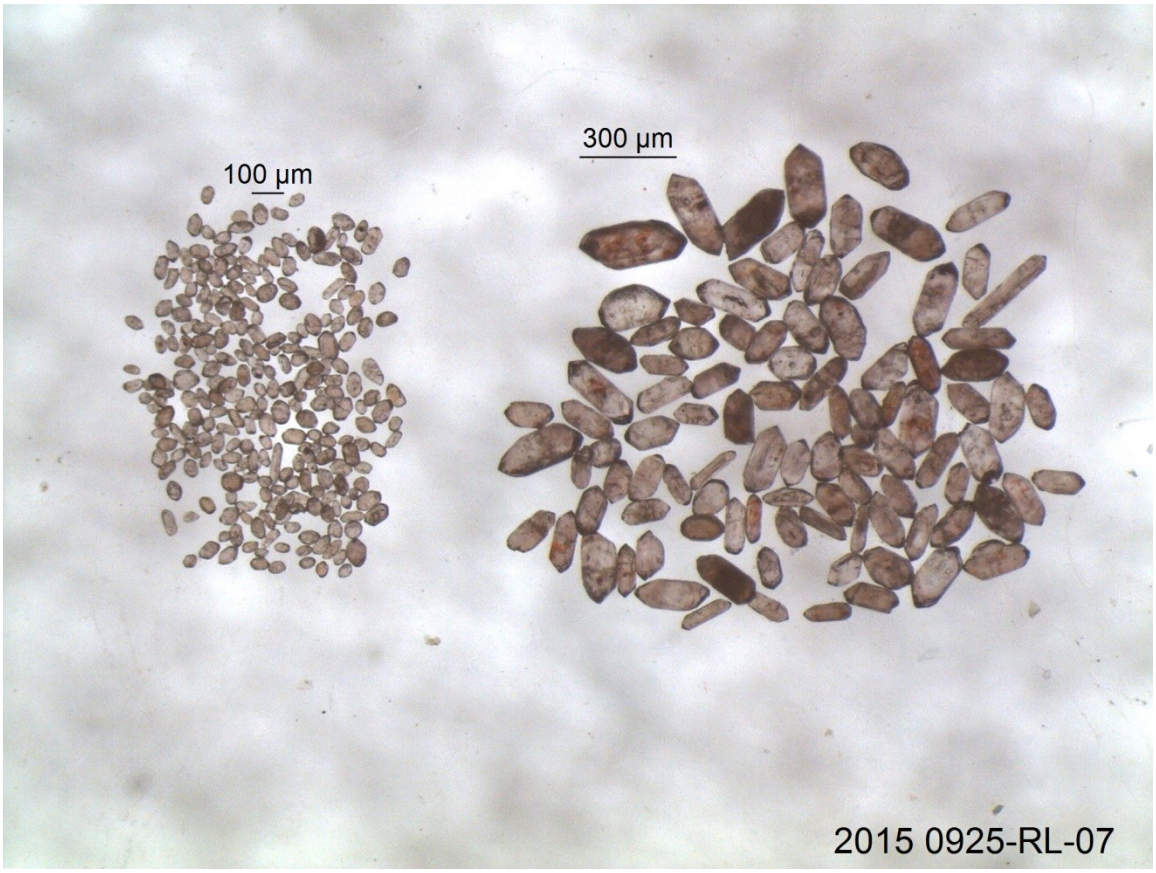

Figure A3-1. Representative zircons recovered from the French Rocks tonalite, 20150925RL-07. There appears to be a bimodal distribution of grain sizes. Subpopulations of each size were processed separately to test for any differences in U-Pb ages.

Figure A3-2. Examples of partially dissolved zircons after the first step of chemical abrasion. High-uranium domains and crystal defects are preferentially dissolved in the first step, thereby removing the most metamict portions of the grains, which typically have the most Pb loss and highest concentrations of labile common Pb. Individual partially dissolved zircons and zircon fragments were selected, spiked with ET535 U-Pb isotopic tracer, completely dissolved and analyzed for U-Pb data.

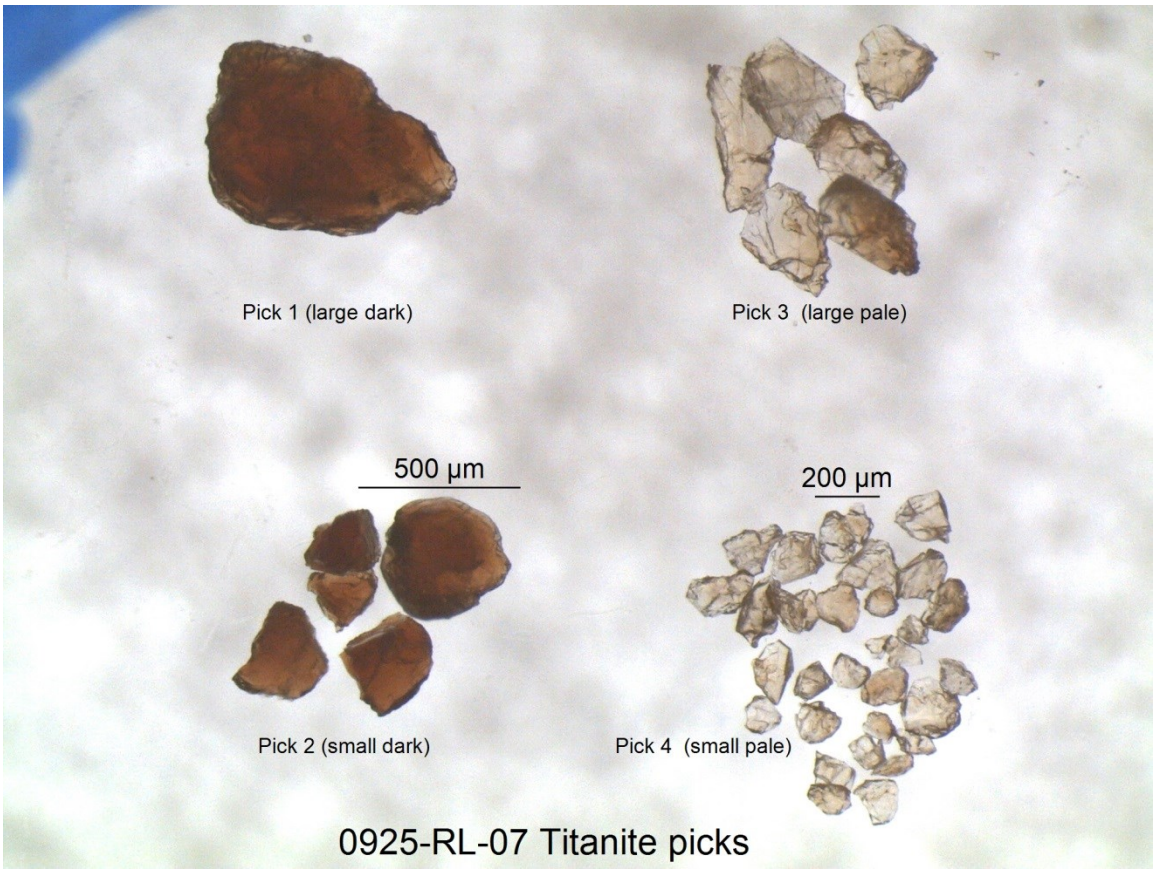

Figure A3-3. Four picks of titanite dated by dissolution and ID-TIMS. Dark titanite grains typically grow at higher temperatures than pale grains (Frost and others, 2000). Size ranges of each colored population were also selected to test for any potential diffusive Pb loss due to cooling. Closure temperatures for Pb diffusion in titanite are ca. 650 to 750°C (Frost and others, 2000), but can vary with effective diffusive diameter.

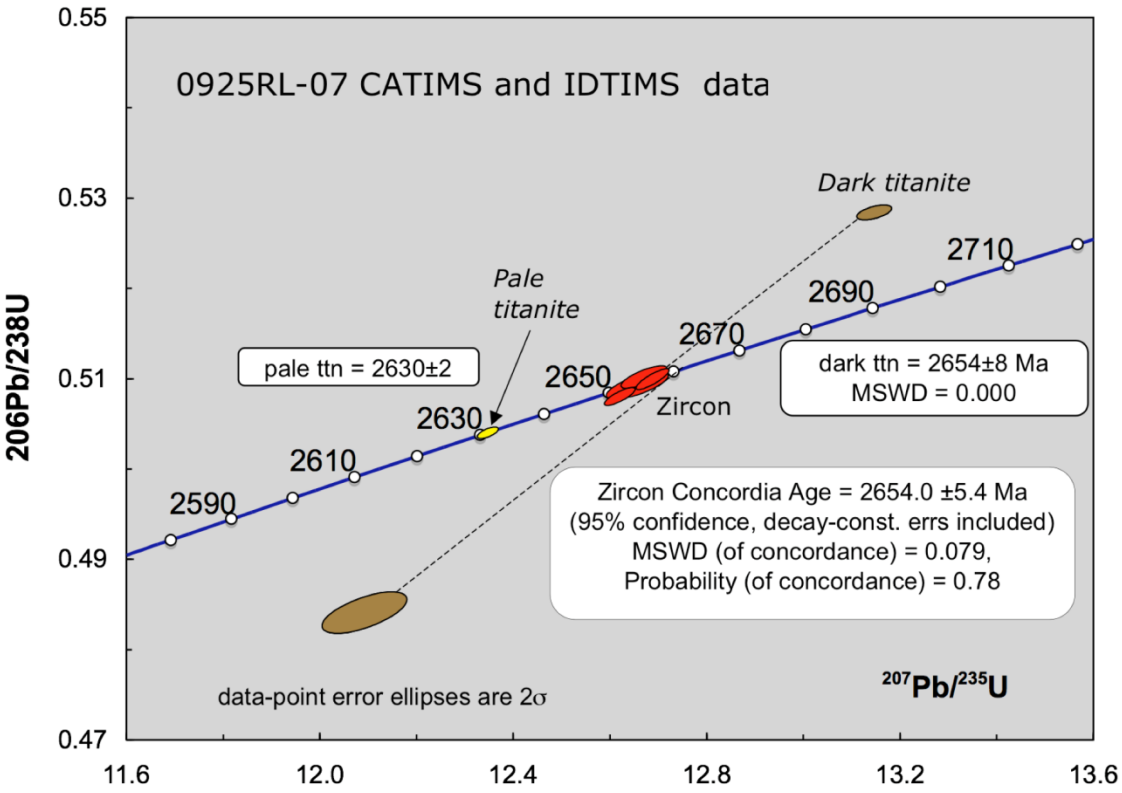

Figure A3-4. Concordia plot of zircon and titanite data from French Rocks tonalite, 20150925RL-07. The four single-grain zircon CA-TIMS analyses (red ellipses) overlap each other and concordia and produce a Concordia Age of 2,654±5 Ma. Data from two analyses of dark titanite (brown ellipses) display variable disturbances of the U-Pb system, but their $^{207}Pb/^{206}Pb$ dates (dashed line projections) overlap the zircon Concordia Age. The pale titanite data (yellow ellipse) are concordant and distinctly younger.

Table A3-1. Sample 20150925RL-07, CATIMS U-Pb zircon and IDTIMS titanite data, 2,655.0±2.5 Ma weighted mean $^{207}Pb/^{206}Pb$ date, 4 zircons, MSWD 1.6. sample: z=zircon, sph=titanite, sm=small, lg=large, dk=dark, pa=pale, s=single grain, tip=zircon grain tip, p=pick identifier, gr=number of grains. Weight: titanite weights are accurate, but zircon weights represents an estimate after first step of CATIMS zircon dissolution and is only approximate. U and Pb concentrations are based on this weight and are useful for internal comparisons only. Picograms (pg) sample and common Pb from the second dissolution step are measured directly, however and are accurate. Sample Pb: sample Pb (radiogenic + initial) corrected for laboratory blank. All common Pb from zircons was assigned to blank; 4 picograms for titanite. cPb: total common Pb. Pb*/Pbc: radiogenic Pb to total common Pb (blank + initial). Corrected atomic ratios: $^{206}Pb/^{204}Pb$ corrected for mass discrimination and tracer, all others corrected for blank, mass discrimination, tracer and initial Pb, values in parentheses are 2 sigma errors in percent. Rho: $^{206}Pb/^{238}U$ versus $^{207}Pb/^{235}U$ error correlation coefficient nd: not determined. Pb isotope dilution data was uninterpretable, underspiked. Zircon and titanite dissolution and chemistry were adapted from methods developed by Krogh (1973), Tilton (1973), Parrish and others (1987), and Mattinson (2005). All zircons were chemically abraded (CATIMS). Final dissolutions were spiked with a mixed $^{205}Pb/^{233}U/^{235}U$ tracer (ET535). Pb and UO_2 from zircons were loaded onto single rhenium filaments with silica gel without any ion exchange cleanup. Titanite grains were spiked with ET535, dissolved in HCl and HF, and purified on HCl-HBr ion exchange columns. Pb from titanite was loaded onto single rhenium filaments with silica gel, U from titanite was loaded separately with graphite and run as a metal. Isotopic compositions were measured in single Daly-photomultiplier mode for zircon and static multi-collector Faraday or Daly/Faraday mode for titanite on a Micromass Sector 54 thermal ionization mass spectrometer at the University of Wyoming. Mass discrimination for Pb was 0.245±0.10 %/amu for Daly analyses and 0.100±0.06% for Faraday analyses based on replicate analyses of NIST SRM 981. U fractionation was determined internally during each run. Procedural blanks ranged from 3 to 0.44 pg Pb during the course of the study. U blanks were consistently less than 0.1 pg. Isotopic composition of the Pb blank was measured as 18.425±0.65, 15.595±0.63, and 36.969±1.08 for 206/204, 207/204 and 208/204, respectively. Concordia coordinates, intercepts, uncertainties and Concordia Ages were calculated using MacPBDAT and ISOPLOT programs (based on Ludwig 1988, 1991, 1998); initial Pb isotopic compositions for zircon and dark titanite were estimated as 13.749, 14.90, 33.469 with slightly elevated 207/204 from Stacey and Kramers (1975) model for 2,650 Ma; initial Pb isotopic compositions for pale titanite were estimated as 13.797, 15.01, 33.513 with slightly elevated 207/204 from Stacey and Kramers (1975) model for 2,630 Ma. The decay constants used by MacPBDAT are those recommended by the I.U.G.S. Subcommission on Geochronology (Steiger and Jäger, 1977): 0.155125 x 10-9/yr for 238U, 0.98485 x 10-9/yr for 235U and present-day $^{238}U/^{235}U = 137.88$.

							Corrected atomic ratios												
	Weight	U		sample Pb	cPb	Pb*	Th	^{206}Pb	^{208}Pb	$^{206}Pb/^{238}U$		$^{207}Pb/^{235}U$			$^{207}Pb/^{206}Pb$	206/238	207/235	207/206		Rho
Sample	(µg)	(ppm)	(ppm)	(pg)	(pg)	Pbc	U	^{204}Pb	^{206}Pb	(rad.)	%err	(rad.)	%err	(rad.)	%err	Age (Ma)	Age (Ma)	Age (Ma)	err	
z sm sC	0.34	97	59.9	20	0.7	27.8	0.79	1495	0.22	0.51022	(0.20)	12.6680	(0.31)	0.1801	(0.20)	2657.6	2655	2653.5	±3.4	0.76
z lg sA	7.20	99	59.1	425	3.5	122.0	0.66	6685	0.18	0.50807	(0.17)	12.6172	(0.2)	0.1801	(0.1)	2648.4	2652	2653.9	±2.0	0.81
z sE tip	0.54	232	141.5	76	3.4	22.3	0.76	1216	0.21	0.50934	(0.25)	12.6527	(0.41)	0.1802	(0.29)	2653.8	2654	2654.4	±4.8	0.72
z sF tip	0.54	163	98.5	53	0.4	119.5	0.70	6488	0.19	0.51000	(0.18)	12.6857	(0.22)	0.1804	(0.12)	2656.6	2657	2656.6	±1.9	0.84
dark titanite: 2657±3 Ma weighted mean $^{207}Pb/^{206}Pb$ date, MSWD 2.1																				
sph lg dk p1 1gr	196	118	151.3	29652	4414	5.7	4.56	168	1.22	0.52860	(0.13)	13.1463	(0.22)	0.1804	(0.19)	2735.6	2690	2656.3	±3.1	0.56
sph sm dk p2 5gr	108	172	287.3	31120	11355	1.7	4.64	58	1.36	0.48431	(0.39)	12.0875	(0.59)	0.1810	(0.45)	2546.0	2611	2662.2	±7.5	0.64
pale ttn: 2630±2 Ma weighted mean $^{207}Pb/^{206}Pb$ date, MSWD 0.15																				
sph lg pa p3 5gr	111	24	14.4	1603	129	11.5	0.27	609	0.07	0.50416	(0.10)	12.3439	(0.16)	0.1776	(0.12)	2631.6	2631	2630.4	±2.0	0.66
sph sm pa p4 29gr	107	25	nd	nd	nd	nd	3.16	48	0.83	nd	nd	nd	nd	0.1774	(0.59)	nd	nd	2628.5	±9.7	nd

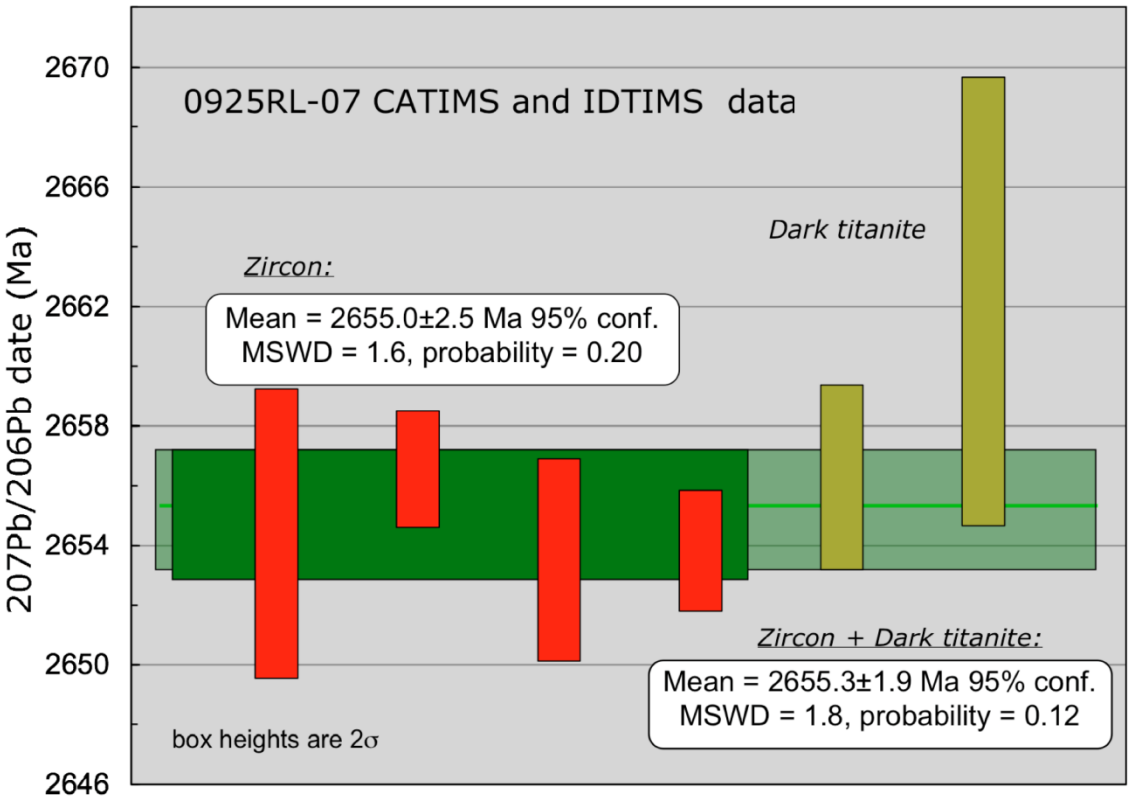

Figure A3-5. Weighted mean plot of $^{207}Pb/^{206}Pb$ dates from four single zircon analyses and two picks of dark titanite. The zircon date of 2,655±2.5 Ma is interpreted as the best estimate for the magmatic age of this sample. The dark titanite dates are consistent with this age and suggest a magmatic origin for the dark titanite grains.

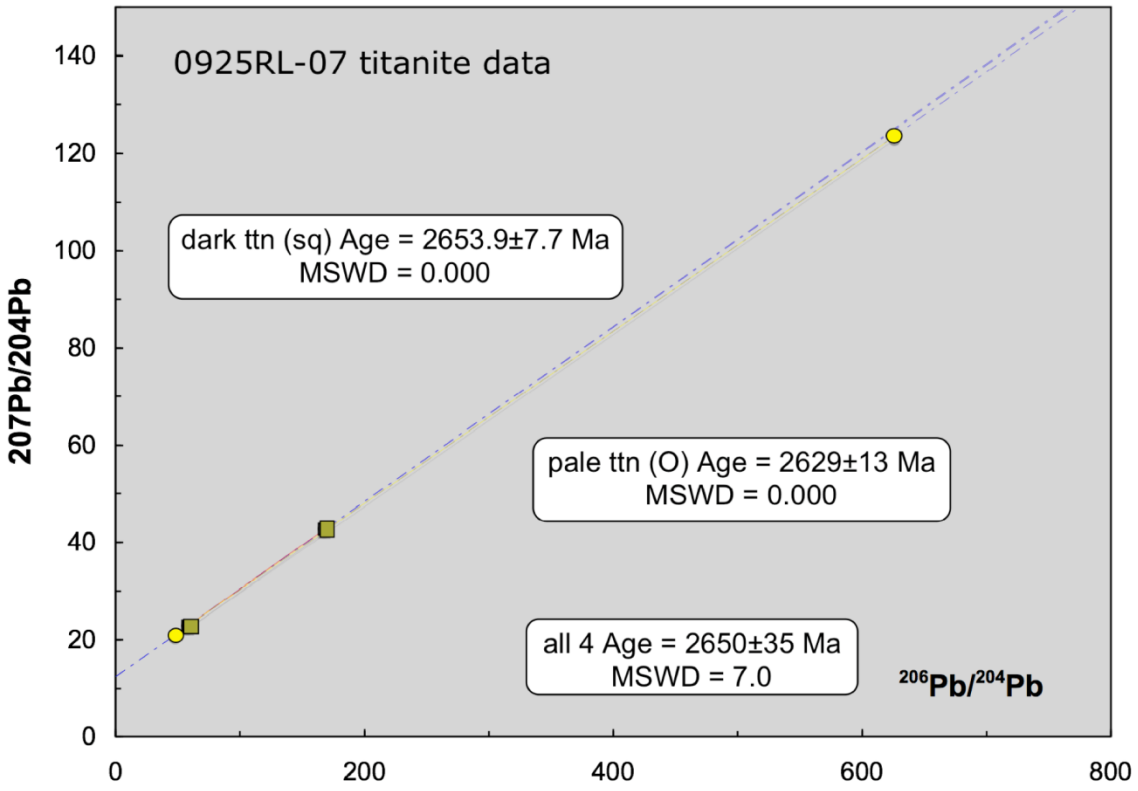

Figure A3-6. Total Pb plot of blank-corrected titanite data. The data include both the radiogenic Pb and the initial, common Pb components in varying mixtures. The dark and pale titanite analyses produce distinctly different $^{207}Pb/^{206}Pb$ dates. The poor MSWD of 7 for a linear regression of all four analyses supports the interpretation that the two colored populations represent different growth ages.

Table A3-2. Sample 20150925RL-07, total Pb IDTIMS titanite data. sample: sph=titanite, lg=large, sm=small, dk=dark, pa=pale, p=pick identifier, gr=number of grains. cPb: common Pb corrected for laboratory blank. Pb*/Pbc: radiogenic Pb to total common Pb (blank + initial). Corrected atomic ratios: corrected for blank, mass discrimination and tracer, values in parentheses are 2 sigma errors in percent. nd: not determined. Pb isotope dilution data was uninterpretable, underspiked. Titanite dissolution and ion exchange chemistry were adapted from methods developed by Tilton (1973) and Parrish and others (1987). Grains were dissolved in HCl with a trace of HF, and were spiked with a mixed $^{205}Pb/^{233}U/^{235}U$ tracer (ET535). Pb and U were purified on HBr/HCl ion exchange columns. Pb and U samples were loaded onto single rhenium filaments with silica gel and graphite, respectively; isotopic compositions were measured in multi-collector, static mode on a Micromass Sector 54 mass spectrometer at the University of Wyoming in Faraday or Daly/Faraday mode. Mass discrimination for Pb was determined by replicate analyses of NIST SRM 981 as 0.100±0.06 %/amu. U fractionation was determined internally during each run. Pb procedural blanks were 4 pg. Isotopic composition of the Pb blank was measured as 18.752±1.04, 15.652±0.60, and 38.810±0.2 for 206/204, 207/204 and 208/204, respectively. U blanks were consistently less than 0.1 pg. Raw data were reduced using MacPBDAT program (based on Ludwig 1988).

								Corrected atomic ratios					
	Weight	U		sample Pb	cPb	Pb*	Th	$^{206}Pb/^{204}Pb$		$^{207}Pb/^{204}Pb$		$^{208}Pb/^{204}Pb$	
Sample	(mg)	(ppm)	(ppm)	(pg)	(pg)	Pbc	U		%err		%err		%err
dark titanite: 2,654±8 Ma two point Pb-Pb isochron, initial 6/4, 7/4 = 13.74, 14.94													
sph lg dk p1 1gr	196	118	151.3	29652	4414	5.7	4.56	167.78	(0.22)	42.6839	(0.31)	222.87	(0.40)
sph sm dk p2 5gr	108	172	287.3	31120	11355	1.7	4.64	58.03	(0.21)	22.9157	(0.30)	95.08	(0.40)
pale titanite: 2,629±13 Ma two point Pb-Pb isochron, initial 6/4, 7/4 = 13.80, 15.01													
sph lg pa p3 5gr	111	24	14.4	1603	129	11.5	0.27	625.81	(1.64)	123.5876	(1.50)	80.78	(2.38)
sph sm pa p4 29gr	107	25	nd	nd	nd	nd	3.16	47.76	(0.21)	21.0344	(0.30)	63.24	(0.40)